Sensitivity of surface temperature to radiative forcing by contrail cirrus in a radiative-mixing model

Ulrich Schumann[1], Bernhard Mayer[2]

[1]Deutsches Zentrum für Luft- und Raumfahrt, Institut für Physik der Atmosphäre, Oberpfaffenhofen, Germany
[2]Ludwig-Maximilians-Universität München, Lehrstuhl für Experimentelle Meteorologie, Munich, Germany

Correspondence to: Ulrich.Schumann@dlr.de

Abstract. Earth's surface temperature sensitivity to radiative forcing (RF) by contrail cirrus and the related RF efficacy relative to CO_2 are investigated in a one-dimensional idealized model of the atmosphere. The model includes energy transport by shortwave (SW) and longwave (LW) radiation and by mixing in an otherwise fixed reference atmosphere (no other feedbacks). Mixing includes convective adjustment and turbulent diffusion, where the latter is related to the vertical component of mixing by large-scale eddies. The conceptual study shows that the surface temperature sensitivity to given contrail RF depends strongly on the time scales of energy transport by mixing and radiation. The time scales are derived for steady layered heating (ghost-forcing) and for a transient contrail cirrus case. The radiative time scales are shortest at the surface and shorter in the troposphere than in the mid-stratosphere. Without mixing, a large part of the energy induced into the upper troposphere by radiation due to contrails or similar disturbances gets lost to space before it can contribute to surface warming. Because of the different radiative forcing at the surface and at top of atmosphere (TOA) and different radiative heating rate profiles in the troposphere, the local surface-temperature sensitivity to stratosphere-adjusted RF is larger for SW than for LW contrail forcing. Without mixing, the surface energy budget is more important for surface warming than the TOA budget. Hence surface warming by contrails is smaller than suggested by the net RF at TOA. Under low mixing conditions, cooling by contrails cannot be excluded. This may in part explain low efficacy values for contrails found in previous global circulation model studies. Possible implications of this study are discussed. Since the results of this study are model dependent, they should be tested with a comprehensive climate model in the future.

Keywords: cirrus, contrail cirrus, radiative forcing, climate change, surface temperature, radiation transfer, mixing, efficacy

1 Introduction

Contrails are similar to upper tropospheric ice clouds (cirrus) which tend to warm the troposphere by reducing outgoing longwave (LW) terrestrial radiation and cool by enhancing shortwave (SW) solar radiation backscattering (Stephens and Webster, 1981; Liou, 1986; Sinha and Shine, 1994; Chen et al., 2000; Schumann and Heymsfield, 2017). For low optical

thickness, the net cloud radiative forcing (RF) from cirrus is often positive at top of the atmosphere (TOA) but negative at the surface (Ackerman et al., 1988; Stackhouse and Stephens, 1991; Fu and Liou, 1993; Jensen et al., 1994; Rossow and Zhang, 1995; Meerkötter et al., 1999; Kvalevåg and Myhre, 2007; Dietmüller et al., 2008; Lee et al., 2009b; Allan, 2011; Berry and Mace, 2014; Hong et al., 2016). For well mixed greenhouse gases, a positive RF implies a global warming (Shine et al., 1994; Hansen et al., 1997a). However, cirrus induces a radiative heat source profile which tends to warm the upper troposphere but may cool the surface (Liou, 1986). Heat induced by radiation in the upper troposphere must be transported downwards to contribute to surface warming, e.g., by convective, baroclinic and other dynamical mixing processes (Manabe and Wetherald, 1967; Stone, 1973; Vallis, 2006). Hence, the question whether cirrus clouds cool or warm the Earth's surface cannot be simply answered from studies of radiative flux changes alone.

The sensitivity of surface temperature to contrail cirrus changes is of relevance with respect to aviation climate impact (Lee et al., 2009a; Boucher et al., 2013; Lund et al., 2017). Long-lived contrails of significant optical thickness (>0.1) are estimated to cover about 0.2 - 0.5 % of the Earth, with higher values in northern mid-latitudes (Minnis et al., 2013; Schumann et al., 2015; Bock and Burkhardt, 2016). Early studies expected a regional surface cooling from contrails (Reinking, 1968). Later, a hemispheric atmosphere warming by contrails was derived from models (Liou et al., 1990). A special report on Global Aviation of the Intergovernmental Panel on Climate Change (IPCC) (Penner et al., 1999) concluded in 1999: "Contrails tend to warm the Earth's surface, similar to high clouds". Observational evidence for contrail-warming is missing because the expected changes are small, not well correlated with contrail cover, and observed changes may have many causes (Minnis, 2005). Contrail RF contributions depend on many contrail and Earth-atmosphere system properties (Meerkötter et al., 1999; Minnis et al., 1999; Myhre and Stordal, 2001; Schumann et al., 2012). Contrails are composed of relatively small and aspherical ice particles (Gayet et al., 2012). Hence, contrails may favor the albedo cooling over the greenhouse warming effect (Fu and Liou, 1993; Strauss et al., 1997; Wyser and Ström, 1998; Zhang et al., 1999; Marquart et al., 2003; Wendisch et al., 2005; Markowicz and Witek, 2011; Bi and Yang, 2017). Contrail contributions to TOA cloud forcings have been derived from observations (Schumann and Graf, 2013; Spangenberg et al., 2013; Vázquez-Navarro et al., 2015). Most traffic occurs during daytime causing contrails with higher SW fraction. The global mean positive LW and negative SW parts may be nearly cancelling each other with a small positive net RF at TOA. Local increases in LW fluxes below contrails are hardly measurable because tropospheric water vapor shields the surface partly from contrail-induced LW flux changes (Kuhn, 1970). Local reductions in SW fluxes are well observable at the surface (Khvorostyanov and Sassen, 1998; Haywood et al., 2009; Weihs et al., 2015). Hence, contrails may have the potential to cool (Sassen, 1997).

The global mean equilibrium change of near-surface air temperature is often approximated by $\Delta T_s = \lambda$ RF as a function of the net downward flux change RF at the tropopause and a "climate sensitivity parameter" λ (Houghton et al., 1990). λ is similar to the planetary temperature sensitivity parameter λ_p to changes in solar irradiance (Stephens, 2005), $\lambda_p = [1/(4 \sigma T_s^3)] (T_s/T_p)^3 [dT_s/dT_p]$. Here σ is the Stefan–Boltzmann constant, T_s is the surface temperature, and T_p is the effective temperature of planetary infrared emissions, $\sigma T_p^4 \cong S_0 (1-a)/4$, with solar irradiance $S_0 \cong 1360$ W m^{-2} and Earth albedo a $\cong$

0.3. Hence, $\lambda_p \cong 0.267$ K W^{-1} m^2 for $[dT_s/dT_p] = 1$. The feedback factor $[dT_s/dT_p]$ differs from one depending on the various forcing types (Stephens, 2005; Bony et al., 2006; Stevens and Bony, 2013). Therefore, λ is not a universal constant (Forster et al., 1997; Joshi et al., 2003; Stuber et al., 2005). The "efficacy" e= λ_c/λ_{CO2}, i.e., the ratio of climate sensitivities λ_c for non-CO_2 disturbances and λ_{CO2} for a given change in CO_2, generally differs from one (Hansen et al., 2005). Various alternative RF definitions have been suggested to improve the link to climate sensitivity (Boucher et al., 2013; Myhre et al., 2013). The instantaneous RF$_i$ is the RF for a fixed atmosphere. The adjusted RF$_a$ is the RF after thermal relaxation of the stratosphere to the disturbance (Houghton et al., 1990; Stuber et al., 2001). The effective RF$_s$ is the RF after adjustment of the atmosphere to disturbances for constant (ocean) surface temperature (Rotstayn and Penner, 2001; Hansen et al., 2002; Shine et al., 2003).

Since air traffic is projected to continue to increase for many decades, it is important to know the climate impact of contrails accurately (Lee et al., 2009a). Various models to represent contrails in three-dimensional atmospheric global circulation models have been developed (Ponater et al., 1996; Rind et al., 2000; Ponater et al., 2002; Marquart et al., 2003; Rap et al., 2010b; Burkhardt and Kärcher, 2011; Jacobson et al., 2011; Olivié et al., 2012; Chen and Gettelman, 2013; Schumann et al., 2015; Bock and Burkhardt, 2016), with different treatments of traffic, subgrid scale contrail formation and optical properties. Some of these models were run with atmosphere-ocean coupling (Rind et al., 2000; Ponater et al., 2005; Rap et al., 2010a; Huszar et al., 2013; Jacobson et al., 2013). The contrail climate effects are expensive to compute because they are small compared to the interannual variability ("climate noise") in climate models (Ponater et al., 1996; Hansen et al., 1997b), so most studies used by factor 10 to 100 increased disturbances. All these model studies suggest a mean global warming from contrails. The contrail efficacy has been computed in a few studies, with results varying from 0.3 to 1 (Hansen et al., 2005; Ponater et al., 2005; Rap et al., 2010a).

The classical RF concept assumes that the surface temperature response follows the TOA energy budget change (Schneider and Dickinson, 1974; Dickinson, 1982). This requires that the energy induced by the disturbance gets well mixed globally within the troposphere and down to the surface. In order to be effective for a long-term ocean warming, the mixing has to occur at time scales fast compared to the time scale of heat loss from the atmosphere to space by radiation. Temperature profile disturbances within the atmosphere relax by thermal relaxation with time scales which are of order hours to months depending, among others, on altitude, vertical disturbance scales, and mixing (Manabe and Strickler, 1964; Zhu, 1993). Mainly because of denser air traffic, most contrails occur at mid-latitudes. At mid-latitudes, mixing is mainly driven by baroclinic instability in the stably stratified, rotating atmosphere, also depending on moisture, leading to large-scale eddies transporting heat from the tropics poleward and upward (Stone, 1973). The baroclinic mixing occurs at time scales of several days (Vallis, 2006). Hence, mixing at mid-latitudes is slower than in convective parts of the tropics where deep convection in clouds causes fast vertical heat transport (Wetherald and Manabe, 1975). Again because of denser traffic, contrails occur mainly over land. It is not sure that the heat induced radiatively by contrails in the troposphere over land reaches the ocean by horizontal advection and downward mixing before getting lost to space by radiation.

In this conceptual study, we investigate changes in temperature from additional thin cirrus (contrails) at mid-latitudes in a radiative-mixing model where the vertical mixing may result from deep convection, from the large-scale circulation, and from turbulent diffusion. For better understanding, the model is run without climate system changes ("feedbacks"; Manabe and Wetherald (1967)) except thermal relaxation by radiation and mixing. The model is run with highly idealized surface conditions (to minimize the number of free parameters), including constant temperature and zero net vertical heat flux at the surface ("adiabatic surface") as bounding extremes. Instead of investigating the approach to equilibrium with ocean coupling, we simulate the equilibrium atmosphere without heat exchange to an underlying compartment. The disturbances considered are small and, hence, change the reference atmosphere only slightly. For this reason the model is run with fixed dynamical heating, simulating the heat sources, e.g., from horizontal heat advection, as required for a steady-state reference atmosphere (Strauss et al., 1997). The optical properties of cirrus are essential for its radiative forcing (Fu, 1996; Myhre et al., 2009; Yang et al., 2015), but for this study, the cirrus is just a source of SW and LW radiation flux-profile changes with cloud-radiation interaction details of secondary relevance. Also, aerosol effects are not included in this study. The method is described in Section 2. Section 3 presents the results. Section 3.1 shows the responses of an idealized atmosphere to prescribed heating, so-called "ghost forcing". This part will point out the importance of the vertical distribution of the radiative heat sources and vertical mixing. The thermal response to a prescribed contrail cirrus layer is studied in Section 3.2. We separate the temperature responses to SW and LW radiative disturbances by contrails and refer correspondingly to "SW cirrus" (similar to layer of small and non-absorbing particles) and "LW cirrus" (similar to a strong greenhouse gas layer). For constant atmosphere, the sum of SW and LW RF from these cirrus versions is the same as the net RF. This part will show different temperature responses to SW and LW radiative forcing. A study of thermal relaxation times for contrail cirrus will show up some consequences of temporally and spatially variable contrails. For comparison and for computation of efficacies for contrails relative to CO_2, we run the same model for changed CO_2. Finally, Section 4 summarizes the approach, the results, and the limitations, and mentions some implications.

2 Radiative-convective-diffusive mixing model

This study uses a one-dimensional radiative-mixing model of the atmosphere with prescribed composition and clouds, following traditional approaches (Möller and Manabe, 1961; Manabe and Strickler, 1964) with turbulent fluxes as in Ramanathan and Coakley (1978).

The model is integrated step-wise in time until steady state. It computes the temperature profile T(z,t) versus altitude z and time t as induced by radiative and turbulent heat transports, based on the heat budget:

$$\rho c_p \frac{\partial T}{\partial t} = -\frac{\partial F_R}{\partial z} - \frac{\partial F_T}{\partial z} + Q_o, \quad F_R = F_{SW}^{up} - F_{SW}^{dn} + F_{LW}^{up} - F_{LW}^{dn}, F_T = -\rho c_p \kappa \left(\frac{\partial T}{\partial z} + \Gamma \right). \tag{1}$$

Here, ρ and c_p are air density and isobaric specific heat capacity, F_R is the net radiative flux (sum of upward and downward SW and LW fluxes), F_T is the turbulent heat flux, Γ is a prescribed threshold lapse rate, and $\kappa=\kappa(t,z)$ is a turbulent diffusivity selected to approximate diffusive mixing (constant κ) or convective adjustment (large κ in case of unstable stratification), as explained below. For contrails and for other small disturbances we compute the temperature change profile $\Delta T(t,z) = T(t,z)-T_0(z)$ in a given reference atmosphere with temperature profile $T_0(z)$, i.e., we run the model with "fixed dynamical heating" Q_0. Here, $Q_0 = \partial(F_R + F_T)/\partial z$ is the divergence of the total flux for $T = T_0$, so that the undisturbed reference atmosphere is steady. Fixed dynamical heating is commonly used for stratospheric adjustment (Ramanathan and Dickinson, 1979; Forster et al., 1997; Myhre et al., 1998). Here we use fixed dynamical heating to study the atmosphere response for a given reference atmosphere to small disturbances (Strauss et al., 1997).

The radiative flux F_R is computed with an efficient delta-Eddington two-stream solver using libRadtran (Mayer and Kylling, 2005; Emde et al., 2016) which is a common solver for climate model applications. Tests with the more accurate discrete ordinate solver DISORT (Stamnes et al., 1998) show flux differences relative to the two-stream solver of about 10 %, mainly in the LW range. Radiation absorption by gases (H_2O, CO_2, O_3, etc.) is calculated with correlated-k distributions for SW (~0.2 - 4 μm) and LW radiation (4 - 70 μm) from Fu and Liou (1992). An alternative SW absorption model from Kato et al. (1999) induces flux differences small compared to those between the two solvers. The model includes a cirrus layer of hexagonal ice crystals with optical properties from Fu (1996) and Fu et al. (1998).

The turbulent flux F_T is approximated as a function of a linearized potential temperature gradient $dT/dz-\Gamma$ including the prescribed lapse rate Γ, and diffusivity κ (Ramanathan and Coakley, 1978; Liou and Ou, 1983). The inclusion of Γ makes sure that an atmosphere under threshold conditions with $dT/dz = -\Gamma$ experiences zero turbulent fluxes. The diffusivity κ is set to zero in the stratosphere and to a constant $\kappa= 100$ m^2 s^{-1} in the troposphere for simulation of diffusive mixing in this study. Liou and Ou (1983) used values up to 200 m^2 s^{-1} to simulate cirrus in the tropical atmosphere. The diffusivity κ causes vertical mixing in the troposphere with time scales L_v^2/κ depending on vertical scales L_v of temperature changes, about 10 d for mixing over the whole troposphere ($L_v \approx 10$ km) and about 3 h for a layer of 1 km depth. Stone (1973) estimates the effective diffusivity κ_H for horizontal mixing by large-scale eddies to be at least 10^6 m^2 s^{-1}. For similar time scales, the diffusivity κ for vertical mixing should be related to κ_H by the square of the ratio of vertical to horizontal length scales. The length scale ratio can be estimated from geostrophic equilibrium, $L_v/L_H \approx f/N$ where f and N are the Coriolis and the Brunt-Väisälä frequencies (Vallis, 2006). For typical mid-latitude and tropospheric values (f= 10^{-4} s^{-1}, N= 0.01 s^{-1}) one obtains $\kappa \approx (L_V/L_H)^2 \kappa_H \approx 100$ m^2 s^{-1}. These are, of course, order of magnitude estimates.

Various methods have been used in the past for "convective adjustment", i.e., enforcement of the lapse rate below a given threshold of, e.g., $\Gamma = 6.5$ K km^{-1} (Manabe and Strickler, 1964; Ramanathan and Coakley, 1978). Here, we increase the diffusivities by the factor 100 $(2/\pi)$ atan(γ), with $\gamma = \max[0,-(\Gamma+dT/dz)/\Gamma_t]$, allowing for a small departure of $-dT/dz$ from the threshold lapse rate Γ by setting Γ_t to 0.1 K km^{-1}. This causes rapid convective adjustment at timescales shorter than one time

step (6 h) and avoids spurious numerical oscillations from the on/off behavior of convection near threshold conditions. The method provides a well-defined turbulent flux, avoids iterations, is numerically stable, and conserves thermal energy.

The numerical scheme uses a non-uniform grid in z with model TOA at 60 km with 100 grid cells vertically. High vertical resolution is necessary to resolve the local flux changes caused by thin cloud layers. The lowest layer is centered at
160   25 m, the highest at 57.5 km, about 0.3 hPa; the grid spacing is $\Delta z = 250$ m between 0.25 and 19 km height. The radiative solver gets the air temperature and composition at grid centers together with the surface temperature as input and returns the fluxes at the grid cell boundaries as output. This staggering avoids 2-Δz-wave artefacts. Diffusive fluxes are computed implicitly with a tridiagonal Gaussian solver based on the temperatures at the next time step. Pressure is recomputed after each change in temperature as a function of altitude for air as ideal gas assuming hydrostatic equilibrium for given
165   gravitational acceleration and surface pressure (1013 hPa). The tropopause is defined by the lowest grid interface with dT/dz > -2 K km^{-1}.

Initial conditions prescribe temperature and composition profiles for the mid-latitude summer standard atmosphere without aerosols (Anderson et al., 1986), see Figure 1. Surface albedo (A = 0.2), solar zenith angle ($\cos(SZA) = 0.6$, SZA=53°) and daytime fraction (0.64) are selected for mid-latitude summer conditions similar to other contrail studies
170   (Meerkötter et al., 1999; Myhre et al., 2009). The 24-h mean TOA fluxes for these conditions are 525, 101 and 298 W m^{-2} for incident solar, reflected solar, and outgoing longwave radiation, respectively. The dynamical heating Q_0 required to keep the mid-latitude summer atmosphere at steady state is shown in Figure 1.

Boundary conditions prescribe either fixed surface temperature or an adiabatic boundary. An adiabatic boundary is implemented by setting $F_R+F_T= 0$ at the surface. This flux is used when computing the heating rate in the lowest model layer.
175   An adiabatic surface implies zero surface heat capacity and zero total flux between the atmosphere above and the compartment below the surface. This condition also simulates an atmosphere in thermal equilibrium with the lower compartment (ocean, ice, etc.). In this study, the surface temperature is set equal to the air temperature T_s in the lowest model layer, implying rapid energy exchange between the surface and the lowest air layer. The code runs stably with 6-h time steps for all applications in this paper.

180   The atmosphere responds to the radiative heating with changes of temperature, see Eq. (1), until the sum of the changed radiative and turbulent fluxes approach a vertically constant value. For constant surface temperature the fluxes stay non-zero. Over an adiabatic surface, the fluxes approach zero at all heights. During integration, we monitor the net vertical flux at all relevant altitudes (during stratospheric adjustment only in the stratosphere). The integration is performed until the maximum deviation of the flux values from the mean at all these altitudes is <0.3 % of the maximum instantaneous flux value.

185   RF is computed from the difference between the net total fluxes in model solutions with and without the disturbance. The sign of RF is defined such that positive values imply a warming of the Earth-troposphere system. The instantaneous (i), stratospheric adjusted (a), and the effective (s) forcing is computed from three model runs with different boundary conditions. RF_i is the flux change for fixed atmosphere; it varies with height. RF_a is the flux change at the tropopause after

the stratosphere temperature has adjusted to the disturbance for fixed troposphere; it is constant throughout the stratosphere. The effective RF_s is the flux change at the tropopause after reaching equilibrium in the entire atmosphere with fixed T_s. Here, the total flux is vertically constant. Finally the equilibrium response is computed for an adiabatic surface for which the total flux change is zero at all levels.

The method has been tested with the mentioned alternative solvers and molecular absorption models by comparison of the daily mean and the time dependent instantaneous SW and LW RF values of a contrail layer with results from earlier studies (Meerkötter et al., 1999); see Figure 2 and Figure 3. For zero dynamical heating, the code reproduces the approach to radiative equilibrium in the atmosphere as in Manabe and Strickler (1964). For a doubled CO_2 mixing ratio (from 300 to 600 µmol mol^{-1}), the model computes a temperature change of 1.1 K without feedbacks, similar to previous results (Hansen et al., 1981).

3 Results and Discussions

3.1 Temperature response to prescribed heating at various altitude levels

In order to understand air and surface temperature responses to heating at various altitudes, we follow the "ghost" forcing concept of Hansen et al. (1997a). The ghost forcing is a prescribed additive flux change causing a constant heating rate in an altitude interval. The heating causes temperature changes until reaching equilibrium in which the changed fluxes balance the ghost forcing. Eleven simulations are performed with a prescribed flux change of 1 W m^{-2}. One simulation is run for a flux change in the lowest model layer above the surface, and ten for flux changes in subsequent 100-hPa pressure intervals between the surface and TOA. The imposed change in net flux is zero at the surface, without direct impact on surface heating, and decreases linearly from 0 to -1 W m^{-2} within the heated atmosphere interval. Above the heated layer, the flux change is constant so that $RF_i = 1$ W m^{-2} at TOA. Because of equal masses, the heating rate H= g $(\partial F_r/\partial p)/c_p = 0.083$ K d^{-1} is constant in the respective 100-hPa intervals, but 0.24 K d^{-1} in the thinner lowest layer for surface ghost forcing. Figure 4 shows, for example, the heating profile for forcing between 600 - 700 hPa. Figure 5 shows the initial and final flux profiles versus height for the disturbances considered in this paper. We find that the flux in equilibrium over a constant-temperature surface is in between the initial instantaneous flux values at the tropopause and at the surface.

Figure 6 shows the steady-state temperature profiles versus pressure-altitude in response to the 11 ghost forcings and for three different versions of vertical mixing; a "radiative case" with zero turbulent fluxes, a "radiative-convective case" with radiative transports and turbulent mixing in unstably stratified layers, and a "radiative-diffusive case" with radiative transport and mixing by constant diffusivity in the troposphere and zero diffusivity in the stratosphere. In the radiative case, the temperature change profiles are similar to vertically smoothed heating rates Here, radiation causes the energy exchange between neighboring layers and between the air layers and the surface (Stephens, 1984; Goody and Yung, 1989). The atmosphere and the surface also emit energy directly to space. Even for ghost forcing at the surface, the lowest air layer gets

warmer than the surface because the warm black surface emits radiation to space more efficiently in the partially transparent thermal infrared window between 8 and 13 μm wavelengths while the air layer's emissivity is lower in this spectral range. In the lower stratosphere, the temperature increase required to balance the ghost forcing is far higher than in the troposphere because of lower emissivity and lower temperature. Turbulent mixing smoothes the profiles further, as expected. Because of stable stratification in the mid-latitude reference atmosphere, convective mixing occurs only in the upper troposphere where the ghost heating is strong enough to cause local instability.

Figure 7a shows the surface temperature change ΔT_s as a function of the height of the heated layer. As expected, ΔT_s is maximum for ghost forcing directly at the surface, $\Delta T_s = 0.37$ K. Above the surface, ΔT_s decreases with the height of the heated layer. So, the ghost forcing efficiency in heating the surface by radiation transfer decreases with layer height. For diffusive mixing, ΔT_s is smaller (0.26 K) and stays close to constant within the whole troposphere. For comparison, Hansen et al. (1997a) (their Table 4 and Fig. 8a) use a coarse-resolution global circulation model and report a vertically nearly constant ΔT_s for fixed clouds, with $\Delta T_s = 0.29$ K when normalized to the same forcing. Apparently their model simulated strong vertical mixing. Small differences were to be expected because of, e.g., different atmospheres.

Figure 7c shows the thermal relaxation time scale $t_R = \Delta T/H$ (in units of days) computed from the steady-state layer-mean temperature change ΔT in the heated layers at various levels and the corresponding heating rate H. For the radiative case, t_R is 0.45 d near the surface (and smaller for thinner surface air layers), 6.6 d in the first 100 hPa layer, 11 d in the upper troposphere, 30 d in the tropopause region between 100 and 200 hPa, and 23 d in the top 100-hPa layer. For layers with 200 hPa depth instead of 100 hPa, the heating response is smoother, causing about 50 % larger time scales. Hence, as expected (Goody and Yung, 1989), the sensitivity to layer depth is less than linear. Radiation causes nonlocal energy transfer, different from diffusion processes for which the sensitivity to layer depth would be quadratic. The smaller time scales in the lowest layers are again a consequence of effective radiation emission via the surface. The relaxation times in the highest layer are lower than in the second highest layer, because of stronger heat loss from the middle atmosphere to space (Zhu, 1993). As expected, mixing reduces the layer warming and the related time scales. Mixing in the troposphere also reduces stratospheric time scales by enhanced heat exchange with and within the troposphere, and enhanced heat loss from the surface to space. With the diffusive mixing, the thermal relaxation times for heating in the troposphere approach a low and vertically constant value of about 3.2 d. For an atmosphere in which the adiabatic surface is replaced by a constant temperature surface, the time scale t_R is zero at the surface; t_R reduces by 34 % in the first 100-hPa layer, and by 12 % in the second layer, with smaller changes at higher levels. In the diffusive case, because of combined transport by radiation and mixing, heat has a lower residence time than a passive tracer with similar source location and constant concentration at the Earth's surface. For comparison, passive aircraft emissions may well exceed one month atmospheric residence time when emitted into the lower stratosphere (Forster et al., 2003) but reach ground within less than about a week when emitted in the mid troposphere (Danilin et al., 1998).

Figure 7b and e show the adjusted and effective RF_a and RF_s versus the height of the heated layer. RF_a equals $RF_i = 1$ W m^{-2}, regardless of the layer height as long as the heated layer is fully below the tropopause (Hansen et al., 1997a). The ratio RF_s/RF_i measures the fraction of heat that warms the compartment below the surface after the air temperature has adjusted to the induced heat disturbance. RF_s/RF_i is largest for heating near the surface: 0.80 without diffusive mixing. Hence, after fast adjustment, when the troposphere has reached its higher steady-state temperature, about 80 % of the input heat heats the compartment below the Earth's surface (e.g., ocean) and 20 % of the heat radiates out to space. For heating near the tropopause, about 95 % of the heat leaves to space. For strong vertical mixing, RF_s/RF_i is about 60 % and vertically nearly uniform. Hence, even with strong mixing, $\sim$40 % of the ghost heating radiates directly to space.

Finally, Figure 7d and f show λ_a and λ_s, the sensitivity parameters of ΔT_s to RF_a and RF_s. For heating at the surface, λ_a = 0.37 K W^{-1} m^2. This value is larger than the planetary sensitivity (0.27 K W^{-1} m^2, without feedbacks) because the atmosphere reduces heat losses from the surface. Without diffusive mixing, the values of λ_a decrease strongly with height, because heating at higher levels is less efficient in radiative surface warming. With diffusive mixing, λ_a approaches a constant because the heating is distributed quickly over the troposphere regardless of the layer height. In contrast, the value of λ_s is close to a constant because RF_s already accounts for the fast temperature profile adjustment. Therefore, as expected (Shine et al., 2003), RF_s is a better measure for surface temperature change than RF_a.

Since ghost forcings change the temperature, they affect LW radiation. The changes depend solely on the temperature profile of the reference atmosphere and the infrared optical properties of the atmosphere and the surface. The solar irradiance is unimportant for fixed dynamical heating. The model response is quasi linear in the magnitude of the disturbances for fixed mixing properties as long as the temperature changes are small compared to absolute temperature. To illustrate the quasi linearity, we tested the model with ghost forcing increased from 1 W m^{-2} to 4 W m^{-2}. The values of t_R for ghost forcing at the surface. e.g., get reduced by up to 0.5 % to 5.7 % for this change, for the three cases, with largest changes for the radiative-convective case. For λ_s, the values range from 0.6 % to 1.2%. Further tests have shown that the basic altitude dependence in the sensitivity to ghost forcing exists also for zero dynamical heating.

We applied the model also for atmospheres with an additional cirrus layer in the upper troposphere, with increased humidity, with increased absolute humidity keeping the relative humidity constant, with increased CO_2, and for other standard atmospheres. All these changes cause changed t_R, RF_s, and temperature sensitivity λ_s values. Clouds of sufficient optical depth above the heated layers reduce the heat loss to space notably. A uniformly higher humidity in the atmosphere enhances the infrared layer emissivity, causing stronger local cooling from a ghost layer to space; it also increases the optical thickness between the layer and the surface, reducing surface temperature changes. This is no contradiction to the fact that increases in stratospheric water vapor (and CO_2) act to cool the stratosphere but to warm the troposphere (Manabe and Wetherald, 1967; Shine and Sinha, 1991; Solomon et al., 2010). In the more humid tropics with higher and colder tropopause, the relaxation time scales are about 20 % smaller than at mid-latitudes. The response to changes for fixed relative humidity helps to understand climate change feedbacks (Manabe and Wetherald, 1967), but requires a more

285 extensive model to be realistic. For an atmosphere with doubled CO_2, the changes are qualitatively similar to increased H_2O, but of smaller magnitude. High and thick clouds are far more efficient in changing the radiative relaxation time scales in the troposphere than added H_2O or CO_2.

3.2 Contrail cirrus in comparison to CO_2

In this section we consider the temperature changes induced by a contrail cirrus example, a thin homogenous cirrus layer at
290 10 to 11 km altitude, with 3 % coverage (typical for mid-latitude contrails) in an otherwise fixed Earth-atmosphere system. The ice water content of the cirrus is adjusted to an optical thickness $\tau = 0.3$ at 550 nm wavelength, and the effective radius of the hexagonal ice particles in this model is set to 20 μm, typical for aged contrails (Minnis et al., 2013; Schumann et al., 2017). At TOA, the net instantaneous RF is positive while the net surface RF_i is negative, consistent with earlier results (see Figure 2). For comparison, we also consider a 10 % increase in CO_2 (360 to 396 μmol mol^{-1}) in the same model. Figure 4
295 and Figure 5 show the instantaneous radiative flux changes and the corresponding heating rates for added SW, LW and "normal" (SW+LW) contrail cirrus and for increased CO_2. Figure 8 shows the steady-state temperature response to the radiative disturbance for the three cirrus cases and CO_2.

For contrail cirrus, we see strongly different temperature responses in the net, SW and LW versions (Figure 8). The SW contrail causes a slight warming inside the cirrus layer by solar radiation absorption (Stackhouse and Stephens, 1991). The
300 main SW effect is a cooling of the lower troposphere culminating at the Earth's surface. The LW contrail enhances infrared absorption inside the layer and slightly warms the troposphere below by emission from the contrail. In addition, the LW contrail enhances the radiation energy budget at the Earth's surface, causing a slight warming, but the SW cooling dominates. In the radiative case, the temperature change is positive in the upper troposphere and negative near the surface. Convective mixing occurs for this atmosphere, with fixed dynamical heating, only in the upper troposphere where the
305 contrail heating causes unstable stratification. The diffusive mixing distributes the heat nearly uniformly over the troposphere. Without such mixing, the heat induced radiatively by the contrail in the upper troposphere is inefficient in heating the surface.

The CO_2 case shows tropospheric warming as expected (Ramanathan and Coakley, 1978; Manabe and Stouffer, 1980; Ogura et al., 2014). The initial heating, mainly from LW radiation, is positive but small (<0.022 K d^{-1}) in the troposphere and
310 negative in the upper stratosphere with far larger magnitude (-0.6 K d^{-1} at 60 km). Enhanced CO_2 not only heats the troposphere, it also increases the downwelling LW flux reaching the surface. For the given atmospheres and disturbances, convective adjustment occurs only in the middle and in the upper troposphere; the other parts remain stably stratified. The literature shows a range of results for CO_2-induced heating rates (Collins et al., 2006; Dietmüller et al., 2016). The larger global mean upper tropospheric temperature response in climate models (Hansen et al., 1997a) results from amplification by
315 various feedbacks not included in this model. Global models often show a rather smooth profile of temperature increase in the troposphere, likely because of strong mixing. At high latitudes, reduced vertical mixing under stably stratified conditions,

besides sea ice albedo changes, is known to cause enhanced LW warming at the surface from increased CO_2 (Wetherald and Manabe, 1975).

Table 1 lists the values for RF_i (at TP, TOA, and surface), RF_a and RF_s at the TP, ΔT_s, and related λ_a, λ_s and efficacy values e_a, e_s, with respect to the CO_2 disturbance, for the radiative and diffusive cases. The instantaneous and stratospheric adjusted values apply to fixed troposphere and are, hence, independent of tropospheric mixing. The results for the radiative-convective case are close to the radiative case and not shown, therefore.

For CO_2, RF_i is positive throughout the atmosphere. RF_a at the tropopause is in between the RF_i values at TOA and at the tropopause, consistent with earlier results (Stuber et al., 2001; Dietmüller et al., 2016). The effective RF_s for fixed climate system is in between the RF_i values at the tropopause and at the surface.

For contrail cirrus, Table 1 shows that RF_a is small and not much different from RF_i, consistent with Dietmüller et al. (2016). The RF_s values differ strongly from RF_a, even with different sign in the radiative case without diffusive mixing. For SW and LW cirrus separately, the ratio $RF_s/RF_{i,TOA}$ increases strongly for diffusive mixing, e.g., from 0.23 to 0.92 for LW cirrus. At steady state, more and more of the heat induced radiatively by the cirrus reaches the surface and less leaves to space for increased mixing. The temperature sensitivity λ_s is about 40 % smaller with the mixing. Surface heating (or cooling) is more efficient in heating the underlying compartment (larger RF_s/RF_i) than upper tropospheric heating. For the LW+SW contrail, the SW and LW results for RF and temperature add linearly. However, the sensitivities and efficacies change nonlinearly because they are ratios of RF and ΔT_s values. Based on RF_a, the efficacy of SW contrail cirrus is larger than for LW contrail cirrus. Hence, efficacies derived from stratosphere-adjusted RF depend on the heating profiles and on the mixing in the troposphere. Based on RF_s, the efficacies for SW and LW contrail cirrus are close to unity. They are all close to one, because the cloud and the CO_2 changes considered are small disturbances of the same climate system and the modelled climate systems remain similar also after fast adjustments in these model cases.

The thin contrail cirrus changes the thermal relaxation properties of the atmosphere only little. It would require a contrail cirrus with optical depth of order one and 100 % cover to cause strong changes of the heat losses to space. Hence, the insight gained for ghost forcing, consistent with Hansen et al. (1997a), helps to understand the temperature changes induced by radiative heating from contrails. For weak mixing, ΔT_s is highly sensitive to the altitude in which the cirrus heating is induced. Also the dependence of λ on mixing and the usefulness of effective RF_s to estimate ΔT_s with nearly constant λ_s found for ghost forcing, apply similarly for cirrus. Similar efficacies can be expected only for similar atmospheres and sufficient vertical mixing. In all cases, we find that the effective RF_s is in between RF_i at the tropopause and at the surface. This finding may be helpful for estimating RF_s for given instantaneous RF.

Different from ghost forcing, the contrails change the optical properties not only in the infrared but also in the solar range. The effects of the contrails are, of course, sensitive to surface albedo and SZA which were irrelevant for ghost forcing. However the model behaves still quasi linearly. An increase of contrail coverage, e.g., from 3 to 12 % changes the

efficacies by 0.38%, 3.87% and -2.76% for SW, LW and SW+LW contrails in the radiative case and by smaller values for the two cases with mixing. Some of the cases were recomputed with DISTUF instead of the more efficient two-stream solver. For CO_2 and SW+LW contrail cirrus, the values in Table 1 differ by <8 % in magnitude between the two solvers.

Ponater et al. (2005) studied contrail climate sensitivity with a global circulation model. They show a plot of the zonal mean vertical cross-section of annual mean temperature response in the equilibrium climate which shows that the contrail-induced warming is largest in the upper troposphere and limited to the latitude band in which contrails formed. The maximum in the upper troposphere cannot be explained by local release of latent heat, because the amount of water condensing during cloud formation at those low-temperature levels is small. The pattern with enhanced temperature for contrails is more pronounced than for a similar CO_2 disturbance simulation (see Figure 1 of Ponater et al. (2006b)). Hence, the mixing was likely not strong enough to disperse the contrail-induced radiative heating uniformly over the troposphere. The different efficacies found by Rap et al. (2010a) and by Ponater et al. (2005) may be caused by different vertical mixing in the different models, besides different ratios of SW to LW RF magnitudes and different feedbacks.

Figure 9 illustrates the timescales of temperature relaxation inside the atmosphere for a non-steady case. Here we show temperature profiles as a function of time starting from steady state for the given contrail cirrus over an adiabatic surface, e.g. over land, after the contrail is suddenly taken away. The times needed to reach half the initial values, derived from plots of the results versus time, are 0.8 d, 8 d, and 50 d for the temperature at the surface, on average in the contrail layer, and in the troposphere, respectively, for the radiative case. The mean tropospheric halving time is 12 d for the radiative-diffusive case. As expected from the ghost forcing results, the temperature change returns to zero most rapid at the surface; the temperature within the contrail layer also returns to zero quickly because of the relatively small geometrical contrail layer depth, while the troposphere in whole needs nearly 2 months to reach half its initial mean value. The larger troposphere value is a consequence of its larger thickness. For constant surface temperature and the diffusive mixing, the troposphere reaches half its initial value after 2.7 d. Of course, thermal inertia of an ocean would increase heat residence times to many years (Hansen et al., 1985). The example illustrates quick losses of energy by radiation to space, which gets enhanced by mixing within the troposphere.

4 Summary, Implications and Conclusions

The surface temperature sensitivity to small climate disturbances has been investigated in an idealized climate model without feedbacks except by temperature changes and lapse-rate dependent convection. The model is a one-dimensional representation of the mid-latitude summer atmosphere with constant insolation. Fixed dynamical heating is imposed to study small disturbances of an undisturbed atmosphere in steady state. The boundary conditions prescribe either fixed surface temperature or zero heat flux through the surface. The fixed-surface-temperature case is used to simulate fast adjustment processes; it provides the effective RF estimate. The zero-heat-flux case simulates an atmosphere in thermal equilibrium with the compartment below the surface. Disturbances considered are layer heating ("ghost forcing"), a prescribed contrail

cirrus layer, and a 10 % increase of CO_2 mixing ratio. Radiative fluxes are computed with an efficient two-stream solver from libRadtran. Diffusive fluxes are driven by the potential temperature gradient. The diffusivity is set either constant or lapse-rate dependent to simulate vertical diffusive mixing, e.g., from large scale eddies, or convective adjustment in unstable layers of the atmosphere. The model response is quasi linear in the magnitude of the disturbances for fixed mixing properties but nonlinear with lapse-rate dependent convective adjustment. From the model results, the ratio of layer-mean temperature changes to heating rates is used to characterize the time scales for radiative relaxation. Model results for various boundary conditions are used to compute instantaneous, stratosphere-adjusted, and effective RF, i.e., RF_i, RF_a, and RF_s.

The model results provide thermal relaxation time scales of the order of hours near the surface, of about one to two weeks in the upper troposphere and of order a month in the lower stratosphere. After fast adjustment, RF_s is nonzero and smaller in magnitude than RF_i. Final thermal equilibrium with an ocean below the surface would be reached far later, after many years to centuries. This final state is simulated with the zero-flux boundary condition. The ratio $RF_s/RF_{i,TOA}$ measure the fraction of the instantaneous energy flux change at TOA available after fast adjustments for long term heating of the compartment below the surface. The ratio RF_s/RF_i depends on the height of where the disturbance induces radiative heating. For zero turbulent mixing, RF_s/RF_i decreases from large values (80 % in the case simulated) for heating directly at the surface to small values (<5 %) above the tropopause. For the diffusive vertical mixing in the troposphere, the ratio RF_s/RF_i approaches a constant of order 60 %. Hence, a large fraction (about 40 %) of the initial energy flux disturbance radiates to space and cannot heat the compartment below the surface. The temperature sensitivity varies with layer height if defined relative to RF_i but is constant relative to RF_s. RF_s controls the transient heating rate of the compartment below the surface.

The contrail layer introduces a positive instantaneous RF at TOA in the LW and a negative RF in the SW range with a small positive net RF. The heating rate profiles in the LW and SW ranges are different with larger magnitude near the surface for SW than for LW flux changes. At the surface, the net RF is negative. As a consequence, the temperature sensitivities differ between the LW and SW forcing parts and change depending on the degree of mixing. For zero mixing, the surface energy budget with SW cooling may dominate the LW warming at the surface. Hence, the temperature sensitivity could be negative.

Taking the temperature sensitivity to the CO_2 disturbance in the same atmosphere for reference, we find that the contrail efficacies based on RF_i differ strongly from unity while those based on RF_s are near one. The temperature sensitivity for the sum of SW and LW RF is the ratio of differences of large opposing values and hence, sensitive to minor system changes. So, for contrails with large and nearly cancelling LW and SW effects, no simple relationship between radiative forcing and temperature change may exist. The findings may apply also for other disturbances.

It is important to keep in mind that the results presented in this study are from a conceptual model. The results are model and case dependent. The fast adjustment and even more the equilibrium responses in general depend on many feedbacks to the temperature-mediated climate system changes, not included in this study. Any change in the model setup, the reference atmosphere or the nature and magnitude of the disturbances would change the results at least quantitatively. Hence, though our study shows the principle importance of mixing for climate sensitivity to contrails, we cannot say how

important mixing is for real world cases quantitatively. Ultimately, this requires careful simulations with a comprehensive climate model.

One climate model study (Ponater et al., 2005) indicates that the mixing of contrail-induced warming may be indeed weak and insufficient to mix the heat over the troposphere uniformly. Differences between the efficacy estimates from various studies may partly be caused by different mixing rates in the models used. Future studies should document the mean radiative, adjective and turbulent energy fluxes, including the TOA and surface energy budgets, to allow for analysis of the relative importance of various energy transport mechanisms for climate sensitivity. It may be of interest whether a correlation between contrails and atmospheric mixing conditions exist. Contrail-induced heating in the upper troposphere during calm weather may contribute less to surface warming than the same forcing in a strongly mixing weather situation. Shorter time scales of SW-induced temperature changes near the surface may lead to a dominance of SW surface cooling relative to LW warming regionally where contrails form, while remaining LW warming may dominate after advection downstream at larger distances. The importance of advection of heat induced by contrail warming has been noted previously (Ponater et al., 1996; Rind et al., 2000), and also for other disturbances (Shindell et al., 2010), but the potential for different radiative warming and cooling effects at different altitudes has not yet been discussed.

These findings may have implications for the assessment of the climate impact of aviation by contrails. So far, equilibrium warming from contrails is computed using estimates of RF (RF_i or RF_a) together with a CO_2 climate sensitivity corrected by a contrail efficacy (Ponater et al., 2006a; Lee et al., 2009a; Frömming et al., 2012). Our study suggests that the efficacy should be different for SW and LW forcings. This may be important for comparison of the climate impact of different contrail cases, e.g., for different diurnal traffic cycles or different route settings.

This study provides further insight into known limitations of the RF model approach. Hence, better approaches are needed. A suggestion for an alternative to the RF concept, based on a new temperature forcing concept, will be described in a follow-on paper (submitted) to this study.

Acknowledgments. Stimulating discussions with Klaus Gierens, Michael Ponater, and Robert Sausen are gratefully acknowledged. Discussions with Markus Rapp, William B. Rossow, Keith Shine, Björn Stevens, Manfred Wendisch and Sebastian Schmidt helped to sharpen the arguments. An invitation by Z. Jonny Luo to the Bill Rossow's retirement symposium in New York in June 2017 triggered part of this research. We thank the reviewers for several comments which lead to improvements of the paper.

References

Ackerman, T. P., K. N. Liou, F. P. J. Valero, and L. Pfister: Heating rates in tropical anvils, J. Atmos. Sci., 45, 1606-1623, 1988.

Allan, R. P.: Combining satellite data and models to estimate cloud radiative effect at the surface and in the atmosphere, Meteorol. Appl., 18, 324-333, doi: 10.1002/met.285, 2011.

450   Anderson, G., S. Clough, F. Kneizys, J. Chetwynd, and E. Shettle: AFGL atmospheric constituent profiles (0-120 km), Tech. Rep. AFGL-TR-86-0110, Air Force Geophys. Lab., Hanscom Air Force Base, Bedford, Mass., 43 pp., 1986.

Berry, E., and G. G. Mace: Cloud properties and radiative effects of the Asian summer monsoon derived from A-Train data, J. Geophys. Res., 119, 9492-9508, doi: 10.1002/2014JD021458, 2014.

Bi, L., and P. Yang: Improved ice particle optical property simulations in the ultraviolet to far-infrared regime, J. Quant. Spectrosc. Radiat. Transf., 189, 228-237, doi: 10.1016/j.jqsrt.2016.12.007, 2017.

455   Bock, L., and U. Burkhardt: Reassessing properties and radiative forcing of contrail cirrus using a climate model, J. Geophys. Res., 121, 9717-9736, doi: 10.1002/2016JD025112, 2016.

Bony, S., R. Colman, V. M. Kattsov, R. P. Allan, C. S. Bretherton, J. L. Dufresne, A. Hall, S. Hallegate, M. M. Holland, W. Ingram, D. A. Randall, B. J. Soden, G. Tseloudis, and M. J. Webb: How well do we understand and evaluate climate feedback processes?, J. Clim., 19, 3345-3348, doi: 10.1175/JCLI3819.1, 2006.

460   Boucher, O., D. Randall, P. Artaxo, C. Bretherton, G. Feingold, P. Forster, V.-M. Kerminen, Y. Kondo, H. Liao, U. Lohmann, P. Rasch, S. K. Satheesh, S. Sherwood, B. Stevens, and X. Y. Zhang: Clouds and Aerosols., in: Climate Change 2013: The Physical Science Basis, edited by: Stocker, T. F., Qin, D., Plattner, G.-K., Tignor, M., Allen, S. K., Boschung, J., Nauels, A., Xia, Y., Bex, V., and Midgley, P. M., Cambridge University Press, Cambridge, United Kingdom and New York, NY, USA, 571-657, 2013.

465   Burkhardt, U., and B. Kärcher: Global radiative forcing from contrail cirrus, Nature Clim. Change, 1, 54-58, doi: 10.1038/NCLIMATE1068, 2011.

Chen, C.-C., and A. Gettelman: Simulated radiative forcing from contrails and contrail cirrus, Atmos. Chem. Phys., 13, 12525–12536, doi: 10.5194/acp-13-12525-2013, 2013.

Chen, T., W. B. Rossow, and Y. C. Zhang: Radiative effects of cloud-type variations, J. Clim., 13, 264-286, 2000.

470   Collins, W. D., V. Ramaswamy, M. D. Schwarzkopf, Y. Sun, R. W. Portmann, Q. Fu, S. E. B. Casanova, J.-L. Dufresne, D. W. Fillmore, P. M. Forster, V. Y. Galin, L. K. Gohar, W. J. Ingram, D. P. Kratz, M.-P. Lefebvre, J. Li, P. Marquet, V. Oinas, Y. Tsushima, T. Uchiyama, and W. Y. Zhong: Radiative forcing by well-mixed greenhouse gases: Estimates from climate models in the Intergovernmental Panel on Climate Change (IPCC) Fourth Assessment Report (AR4), J. Geophys. Res., 111, D14317, doi: 10.1029/2005JD006713, 2006.

475   Danilin, M. Y., D. W. Fahey, U. Schumann, M. J. Prather, J. E. Penner, M. K. W. Ko, D. K. Weisenstein, C. H. Jackman, G. Pitari, I. Köhler, R. Sausen, C. J. Weaver, A. R. Douglass, P. S. Connell, D. E. Kinnison, F. J. Dentener, E. L. Fleming, T. K. Berntsen, I. S. A. Isaksen, J. M. Haywood, and B. Kärcher: Aviation Fuel Tracer Simulation: Model Intercomparison and Implications, Geophys. Res. Lett., 25, 3947 - 3950, 1998.

Dickinson, R. E.: Modeling climate changes due to carbon dioxide increases, in: Carbon Dioxide Review: 1982, edited by: 480   Clark, W. C., Oxford University Press, New York, NY, 101-141, 1982.

Dietmüller, S., M. Ponater, R. Sausen, K.-P. Hoinka, and S. Pechtl: Contrails, natural clouds, and diurnal temperature range, J. Clim., 21, 5061-5075, 10.1175/2008JCLI2255.1, 2008.

Dietmüller, S., P. Jöckel, H. Tost, M. Kunze, C. Gellhorn, S. Brinkop, C. Frömming, M. Ponater, B. Steil, A. Lauer, and J. Hendricks: A new radiation infrastructure for the Modular Earth Submodel System (MESSy, based on version 2.51), Geosci. 485   Model Dev., 9, 2209-2222, doi: 10.5194/gmd-2015-277, 2016.

Emde, C., R. Buras-Schnell, A. Kylling, B. Mayer, J. Gasteiger, U. Hamann, J. Kylling, B. Richter, C. Pause, T. Dowling, and L. Bugliaro: The libRadtran software package for radiative transfer calculations (version 2.0.1), Geosci. Model Dev., 9, 1647-1672, doi: 10.5194/gmd-9-1647-2016, 2016.

Forster, C., A. Stohl, P. James, and V. Thouret: The residence times of aircraft emissions in the stratosphere using a mean 490   emission inventory and emissions along actual flight tracks, J. Geophys. Res., 108, 8524, doi: 10.1029/2002JD002515, 2003.

Forster, P. M., R. S. Freckleton, and K. P. Shine: On aspects of the concept of radiative forcing, Clim. Dyn., 13, 547-560, 1997.

Frömming, C., M. Ponater, K. Dahlmann, V. Grewe, D. S. Lee, and R. Sausen: Aviation-induced radiative forcing and surface temperature change in dependency of the emission altitude, J. Geophys. Res., 117, D19104, doi: 495   10.1029/2012JD018204, 2012.

Fu, Q.: An accurate parameterisation of the solar radiative properties of cirrus clouds for climate models, J. Clim., 9, 2058-2082, 1996.

Fu, Q., and K. N. Liou: On the correlated k-distribution method for radiative transfer in nonhomogeneous atmospheres, J. Atmos. Sci., 49, 2139-2156, 1992.

500 Fu, Q., and K. N. Liou: Parameterization of the radiative properties of cirrus clouds, J. Atmos. Sci., 50, 2008-2025, 1993.

Fu, Q., P. Yang, and W. B. Sun: An accurate parameterization of the infrared radiative properties of cirrus clouds for climate models, J. Clim., 25, 2223–2237, 1998.

Gayet, J.-F., V. Shcherbakov, C. Voigt, U. Schumann, D. Schäuble, P. Jessberger, A. Petzold, A. Minikin, H. Schlager, O. Dubovik, and T. Lapyonok: The evolution of microphysical and optical properties of an A380 contrail in the vortex phase,
505 Atmos. Chem. Phys., 12, 6629-6643, doi: 10.5194/acp-12-6629-2012, 2012.

Goody, R. M., and Y. L. Yung: Atmospheric Radiation - Theoretical Basis, Oxford Univ. Press, 519 pp., 1989.

Hansen, J., M. Sato, and R. Ruedy: Radiative forcing and climate response, J. Geophys. Res., 102, 6831-6684, 1997a.

Hansen, J., G. Russell, A. Lacis, I. Fung, D. Rind, and P. Stone: Climate response times: Dependence on climate sensitivity and ocean mixing, Science, 229, 857-859, doi: 10.1126/science.229.4716.857, 1985.

510 Hansen, J., D. Johnson, A. Lacis, S. Lebedeff, P. Lee, D. Rind, and G. Russell: Climate impact of increasing atmospheric carbon dioxide, Science, 213, 957-966, doi: 10.1126/science.213.4511.957, 1981.

Hansen, J., M. Sato, L. S. Nazarenko, R. Ruedy, A. Lacis, D. Koch, I. Tegen, T. Hall, D. Shindell, B. D. Santer, P. Stone, T. Novakov, L. Thomason, R. Wang, Y. Wang, D. Jacob, S. Hollandsworth, L. Bishop, J. Logan, A. Thompson, R. Stolarski, J. Lean, R. Willson, S. Levitus, J. Antonov, N. Rayner, D. Parker, and J. Christy: Climate forcings in Goddard Institute for
515 Space Studies SI2000 simulations, J. Geophys. Res., 107, 4347, doi: 10.1029/2001JD001143, 2002.

Hansen, J., M. Sato, R. Ruedy, A. Lacis, K. Asamoah, K. Beckford, S. Borenstein, E. Brown, B. Cairns, B. Carlson, B. Curran, S. d. Castro, L. Druyan, P. Etwarrow, T. Ferede, M. Fox, D. Gaffen, J. Glascoe, H. Gordon, S. Hollandsworth, X. Jiang, C. Johnson, N. Lawrence, J. Lean, J. Lerner, K. Lo, J. Logan, A. Luckett, M. P. McCormick, R. McPeters, R. Miller, P. Minnis, I. Ramberran, G. Russell, P. Russell, P. Stone, I. Tegen, S. Thomas, L. Thomason, A. Thompson, J. Wilder, R.
520 Willson, and J. Zawodny: Forcings and chaos in interannual to decadal climate change, J. Geophys. Res., 102, 25679-25720, doi: 10.1029/97JD01495, 1997b.

Hansen, J., M. Sato, R. Ruedy, L. Nazarenko, A. Lacis, G. A. Schmidt, G. Russell, I. Aleinov, M. Bauer, S. Bauer, N. Bell, B. Cairns, V. Canuto, M. Chandler, Y. Cheng, A. Del Genio, G. Faluvegi, E. Fleming, A. Friend, T. Hall, C. Jackman, M. Kelley, N. Kiang, D. Koch, J. Lean, J. Lerner, K. Lo, S. Menon, R. Miller, P. Minnis, T. Novakov, V. Oinas, J. Perlwitz, J.
525 Perlwitz, D. Rind, A. Romanou, D. Shindell, P. Stone, S. Sun, N. Tausnev, D. Thresher, B. Wielicki, T. Wong, M. Yao, and S. Zhang: Efficacy of climate forcings, J. Geophys. Res., 110, D18104, doi: 10.1029/2005JD005776, 2005.

Haywood, J. M., R. P. Allan, J. Bornemann, P. M. Forster, P. N. Francis, S. Milton, G. Rädel, A. Rap, K. P. Shine, and R. Thorpe: A case study of the radiative forcing of persistent contrails evolving into contrail-induced cirrus, J. Geophys. Res., 114, D24201, doi: 10.1029/2009JD012650, 2009.

530 Hong, Y., G. Liu, and J.-L. F. Li: Assessing the radiative effects of global ice clouds based on CloudSat and CALIPSO measurements, J. Clim., 29, 7651-7674, doi: 10.1175/JCLI-D-15-0799.1, 2016.

Houghton, J. T., G. J. Jenkins, and J. J. Ephraums, Ed.: Climate Change - The IPCC Scientific Assessment, Serial Climate Change - The IPCC Scientific Assessment, Serial, edited by, Intergovernmental Panel on Climate Change, Cambridge University Press, Cambridge, 410 pp., 1990.

535 Huszar, P., H. Teyssèdre, M. Michou, A. Voldoire, D. J. L. Olivié, D. Saint-Martin, D. Cariolle, S. Senesi, D. S. Y. Melia, A. Alias, F. Karcher, P. Ricaud, and T. Halenka: Modeling the present and future impact of aviation on climate: an AOGCM approach with online coupled chemistry, Atmos. Chem. Phys., 13, 10027–10048, doi: 10.5194/acp-13-10027-2013, 2013.

Jacobson, M. Z., J. T. Wilkerson, A. D. Naiman, and S. K. Lele: The effects of aircraft on climate and pollution. Part I: Numerical methods for treating the subgrid evolution of discrete size- and composition-resolved contrails from all
540 commercial flights worldwide, J. Comp. Phys., 230, 5115-5132, doi: 10.1016/j.jcp.2011.03.031, 2011.

Jacobson, M. Z., J. T. Wilkerson, A. D. Naiman, and S. K. Lele: The effects of aircraft on climate and pollution. Part II: 20-year impacts of exhaust from all commercial aircraft worldwide treated individually at the subgrid scale, Faraday Discussions, 165, 369-382, doi: 10.1039/c3fd00034f, 2013.

Jensen, E. J., S. Kinne, and O. B. Toon: Tropical cirrus cloud radiative forcing: Sensitivity studies, Geophys. Res. Lett., 21,
545 2023-2026, doi: 10.1029/94GL01358, 1994.

Joshi, M., K. Shine, M. Ponater, N. Stuber, R. Sausen, and L. Li: A comparison of climate response to different radiative forcings in three general circulation models: Towards an improved metric of climate change, Clim. Dyn., 20, 843-854, doi: 10.1007/s00382-003-0305-9, 2003.

550 Kato, S., T. P. Ackerman, J. H. Mather, and E. E. Clothiaux: The k-distribution method and correlated-k approximation for a shortwave radiative transfer model, J. Quant. Spectrosc. Radiat. Transf., 62, 109-121, 1999.

Khvorostyanov, V., and K. Sassen: Cloud model simulation of a contrail case study: Surface cooling against upper tropospheric warming, Geophys. Res. Lett., 25, 2145-2148, 1998.

Kuhn, P. M.: Airborne observations of contrail effects on the thermal radiation budget, J. Atmos. Sci., 27, 937-943, 1970.

Kvalevåg, M. M., and G. Myhre: Human impact on direct and diffuse solar radiation during the industrial era, J. Clim., 20, 555 4874-4883, doi: 10.1175/JCLI4277.1, 2007.

Lee, D. S., D. W. Fahey, P. M. Forster, P. J. Newton, R. C. N. Wit, L. L. Lim, B. Owen, and R. Sausen: Aviation and global climate change in the 21st century, Atmos. Env., 43, 3520-3537, doi: 10.1016/j.atmosenv.2009.04.024, 2009a.

Lee, J., P. Yang, A. E. Dessler, B.-C. Gao, and S. Platnick: Distribution and radiative forcing of tropical thin cirrus clouds, J. Atmos. Sci., 66, 3721-3731, doi: 10.1175/2009JAS3183.1, 2009b.

560 Liou, K.-N., and S.-C. S. Ou: Theory of equilibrium temperatures in radiative-turbulent atmospheres, J. Atmos. Sci., 40, 214-229, 1983.

Liou, K. N.: Influence of cirrus clouds on weather and climate processes: A global perspective, Mon. Wea. Rev., 114, 1167-1199, 1986.

Liou, K. N., S. C. Ou, and G. Koenig: An investigation of the climatic effect of contrail cirrus. In: Air Traffic and the 565 Environment – Background, Tendencies and Potential Global Atmospheric Effects. U. Schumann (Ed.), Lecture Notes in Engineering, Springer Berlin, 154-169, 1990.

Lund, M. T., B. Aamaas, T. Berntsen, L. Bock, U. Burkhardt, J. S. Fuglestvedt, and K. P. Shine: Emission metrics for quantifying regional climate impacts of aviation, Earth Syst. Dynam., 8, 547–563, doi: 10.5194/esd-8-547-2017, 2017.

Manabe, S., and R. F. Strickler: Thermal equilibrium of the atmosphere with a convective adjustment, J. Geophys. Res., 21, 570 361-385, 1964.

Manabe, S., and R. T. Wetherald: Thermal equilibrium of the atmosphere with a given distribution of relative humidity, J. Atmos. Sci., 24, 241-259, 1967.

Manabe, S., and R. J. Stouffer: Sensitivity of a global climate model to an increase of CO_2 concentration in the atmosphere, J. Geophys. Res., 85, 5529, 1980.

575 Markowicz, K. M., and M. Witek: Sensitivity study of global contrail radiative forcing due to particle shape, J. Geophys. Res., 116, D23203, doi: 10.1029/2011JD016345, 2011.

Marquart, S., M. Ponater, F. Mager, and R. Sausen: Future development of contrail cover, optical depth and radiative forcing: Impacts of increasing air traffic and climate change, J. Clim., 16, 2890-2904, 2003.

Mayer, B., and A. Kylling: The libRadtran software package for radiative transfer calculations: Description and examples of 580 use, Atmos. Chem. Phys., 5, 1855-1877, doi: 10.5194/acp-5-1855-2005, 2005.

Meerkötter, R., U. Schumann, P. Minnis, D. R. Doelling, T. Nakajima, and Y. Tsushima: Radiative forcing by contrails, Ann. Geophysicae, 17, 1080-1094, doi: 10.1007/s00585-999-1080-7, 1999.

Minnis, P.: Reply, J. Clim., 18, 2783-2784, 2005.

Minnis, P., U. Schumann, D. R. Doelling, K. Gierens, and D. W. Fahey: Global distribution of contrail radiative forcing, 585 Geophys. Res. Lett., 26, 1853 - 1856, doi: 10.1029/1999GL900358, 1999.

Minnis, P., S. T. Bedka, D. P. Duda, K. M. Bedka, T. Chee, J. K. Ayers, R. Palikonda, D. A. Spangenberg, K. V. Khlopenkov, and R. Boeke: Linear contrail and contrail cirrus properties determined from satellite data, Geophys. Res. Lett., 40, 3220-3226, doi: 10.1002/grl.50569, 2013.

Möller, F., and S. Manabe: Über das Strahlungsgleichgewicht der Atmosphäre, Z. Meteorol., 15, 3-8, 1961.

590 Myhre, G., and F. Stordal: On the tradeoff of the solar and thermal infrared impact of contrails, Geophys. Res. Lett., 28, 3119-3122, doi: 10.1029/2001GL013193, 2001.

Myhre, G., E. J. Highwood, K. P. Shine, and F. Stordal: New estimates of radiative forcing due to well mixed greenhouse gases, Geophys. Res. Lett., 26, 2715-2718, doi: 10.1029/98GL01908, 1998.

Myhre, G., M. Kvalevag, G. Rädel, J. Cook, K. P. Shine, H. Clark, F. Karcher, K. Markowicz, A. Karda, O. Wolkenberg, Y.
595   Balkanski, M. Ponater, P. Forster, A. Rap, and R. Rodriguez de Leon: Intercomparison of radiative forcing calculations of stratospheric water vapour and contrails, Meteorol. Z., 18, 585-596, doi: 10.1127/0941-2948/2009/0411, 2009.

Myhre, G., D. Shindell, F.-M. Bréon, W. Collins, J. Fuglestvedt, J. Huang, D. Koch, J.-F. Lamarque, D. Lee, B. Mendoza, T. Nakajima, A. Robock, G. Stephens, T. Takemura, and H. Zhang: Anthropogenic and natural radiative forcing, in: Climate Change 2013: The Physical Science Basis. Contribution of Working Group I to the Fifth Assessment Report of the
600   Intergovernmental Panel on Climate Change, edited by: Stocker, T. F., Qin, D., Plattner, G.-K., Tignor, M., Allen, S. K., Boschung, J., Nauels, A., Xia, Y., Bex, V., and Midgley, P. M., Cambridge University Press, Cambridge, United Kingdom and New York, NY, USA., 659-740, 2013.

Ogura, T., M. J. Webb, M. Watanabe, F. H. Lambert, Y. Tsushima, and M. Sekiguchi: Importance of instantaneous radiative forcing for rapid tropospheric adjustment, Clim. Dyn., 43, 1409–1421, doi: 10.1007/s00382-013-1955-x, 2014.

605   Olivié, D. J. L., D. Cariolle, H. Teyssèdre, D. Salas, A. Voldoire, H. Clark, D. Saint-Martin, M. Michou, F. Karcher, Y. Balkanski, M. Gauss, O. Dessens, B. Koffi, and R. Sausen: Modeling the climate impact of road transport, maritime shipping and aviation over the period 1860–2100 with an AOGCM, Atmos. Chem. Phys., 12, 1449-1480, doi: 10.5194/acp-12-1449-2012, 2012.

Penner, J. E., D. H. Lister, D. J. Griggs, D. J. Dokken, and M. McFarland: Aviation and the Global Atmosphere – A Special
610   Report of IPCC Working Groups I and III. Intergovernmental Panel on Climate Change, Cambridge University Press, 365 pp., 1999.

Plass, G. N., G. W. Kattawar, and F. E. Catchings: Matrix operator theory of radiative transfer. 1: Rayleigh scattering, Appl. Opt., 12, 314-329, doi: 10.1364/AO.12.000314 1973.

Ponater, M., S. Marquart, and R. Sausen: Contrails in a comprehensive global climate model: Parameterization and radiative
615   forcing results, J. Geophys. Res., 107, 4164, 10.1029/2001JD000429, 2002.

Ponater, M., S. Brinkop, R. Sausen, and U. Schumann: Simulating the global atmospheric response to aircraft water vapour emissions and contrails. - A first approach using a GCM, Ann. Geophys., 14, 941-960, 1996.

Ponater, M., S. Marquart, R. Sausen, and U. Schumann: On contrail climate sensitivity, Geophys. Res. Lett., 32, L10706, 10.1029/2005gl022580, 2005.

620   Ponater, M., S. Pechtl, R. Sausen, U. Schumann, and G. Hüttig: Potential of the cryoplane technology to reduce aircraft climate impact: A state-of-the-art assessment, Atmos. Env., 40, 6928-6944, doi: 10.1016/j.atmosenv.2006.06.036, 2006a.

Ponater, M., V. Grewe, R. Sausen, U. Schumann, S. Pechtl, E. J. Highwood, and N. Stuber: Climate sensitivity of radiative impacts from transport systems, in: Proceedings of an International Conference on Transport, Atmosphere and Climate (TAC), edited by: Sausen, R., Blum, A., Lee, D. S., and Brüning, C., University of Manchester and DLR Oberpfaffenhofen,
625   http://elib.dlr.de/54467/, 190-196, 2006b.

Ramanathan, V., and J. A. Coakley: Climate modeling through radiative-convective models, Rev. Geophys., 16, 465-489, 1978.

Ramanathan, V., and R. E. Dickinson: The role of stratospheric ozone in the zonal and seasonal radiative energy balance of the Earth-troposphere system, J. Atmos. Sci., 36, 1084-1104, 1979.

630   Rap, A., P. M. Forster, J. M. Haywood, A. Jones, and O. Boucher: Estimating the climate impact of linear contrails using the UK Met Office climate model, Geophys. Res. Lett., 37, L20703, doi: 10.1029/2010GL045161, 2010a.

Rap, A., P. M. Forster, A. Jones, O. Boucher, J. M. Haywood, N. Bellouin, and R. R. D. Leon: Parameterization of contrails in the UK Met Office Climate Model, J. Geophys. Res., 115, D10205, doi: 10.1029/2009JD012443, 2010b.

Reinking, R.: Insolation reduction by contrails, Weather, 23, 171-173, 1968.

635   Rind, D., P. Lonergan, and K. Shah: Modeled impact of cirrus cloud increases along aircraft flight paths, J. Geophys. Res., 105, 19927-19940, doi: 10.1029/1999JD901160, 2000.

Rossow, W. B., and Y.-C. Zhang: Calculation of surface and top of atmosphere radiative fluxes from physical quantities based on ISCCP data sets. Part 2: Validation and first results, J. Geophys. Res., 100, 1167-1197, 1995.

Rotstayn, L. D., and J. E. Penner: Indirect aerosol forcing, quasi forcing, and climate response, J. Clim., 14, 2960-2975,
640   2001.

Sassen, K.: Contrail-cirrus and their potential for regional climate change, Bull. Amer. Meteorol. Soc., 78, 1885-1903, 1997.

Schneider, S. H., and R. E. Dickinson: Climate modeling, Rev. Geophys. Space Phys., 12, 447-493, 1974.

Schumann, U., and K. Graf: Aviation-induced cirrus and radiation changes at diurnal timescales, J. Geophys. Res., 118, 2404-2421, doi: 10.1002/jgrd.50184, 2013.

645 Schumann, U., and A. Heymsfield: On the lifecycle of individual contrails and contrail cirrus, Meteor. Monogr., 58, 3.1-3.24, doi: 10.1175/AMSMONOGRAPHS-D-16-0005.1, 2017.

Schumann, U., B. Mayer, K. Graf, and H. Mannstein: A parametric radiative forcing model for contrail cirrus, J. Appl. Meteorol. Clim., 51, 1391-1406, doi: 10.1175/JAMC-D-11-0242.1, 2012.

Schumann, U., J. E. Penner, Y. Chen, C. Zhou, and K. Graf: Dehydration effects from contrails in a coupled contrail-climate

650 model, Atmos. Chem. Phys., 15, 11179-11199, doi: 10.5194/acp-15-11179-2015, 2015.

Schumann, U., R. Baumann, D. Baumgardner, S. T. Bedka, D. P. Duda, V. Freudenthaler, J.-F. Gayet, A. J. Heymsfield, P. Minnis, M. Quante, E. Raschke, H. Schlager, M. Vázquez-Navarro, C. Voigt, and Z. Wang: Properties of individual contrails: A compilation of observations and some comparisons, Atmos. Chem. Phys., 17, 403-438, doi: 10.5194/acp-17-403-2017, 2017.

655 Shindell, D., M. Schulz, Y. Ming, T. Takemura, G. Faluvegi, and V. Ramaswamy: Spatial scales of climate response to inhomogeneous radiative forcing, J. Geophys. Res., 115, D19110, doi: 10.1029/2010JD014108, 2010.

Shine, K. P., and A. Sinha: Sensitivity of the Earth's climate to height-dependent changes in the water vapour mixing ratio, Nature, 354, 382-384, doi: 10.1038/354382a0, 1991.

Shine, K. P., J. Cook, E. J. Highwood, and M. M. Joshi: An alternative to radiative forcing for estimating the relative

660 importance of climate change mechanisms, Geophys. Res. Lett., 30, 2047, doi: 10.1029/2003GL018141, 2003.

Shine, K. P., Y. Fouquart, V. Ramaswamy, S. Solomon, and J. Srinivasan: Radiative Forcing, in: Climate Change 1994: Radiative Forcing of Climate Change and An Evaluation of the IPCC IS92 Emission Scenarios, edited by: Houghton, J. T., Filho, L. G. M., Bruce, J., Lee, H., Callander, B. A., Haites, E., Harris, N., and Maskell, K., Cambridge University Press, UK, 164-203, 1994.

665 Sinha, A., and K. P. Shine: A one-dimensional study of possible cirrus cloud feedbacks, J. Clim., 7, 158-173, 1994.

Solomon, S., K. H. Rosenlof, R. W. Portmann, J. S. Daniel, S. M. Davis, T. J. Sanford, and G.-K. Plattner: Contributions of stratospheric water vapor to decadal changes in the rate of global warming, Science, 327, 1219-1223, doi: 10.1126/science.1182488, 2010.

Spangenberg, D. A., P. Minnis, S. T. Bedka, R. Palikonda, D. P. Duda, and F. G. Rose: Contrail radiative forcing over the

670 Northern Hemisphere from 2006 Aqua MODIS data, Geophys. Res. Lett., 40, 595-600, doi: 10.1002/grl.50168, 2013.

Stackhouse, P. W., and G. L. Stephens: A theoretical and observational study of the radiative properties of cirrus: Results from FIRE 1986, J. Atmos. Sci., 48, 2044-2059, 1991.

Stamnes, K., S. Tsay, W. Wiscombe, and K. Jayaweera: A numerically stable algorithm for discrete-ordinate-method radiative transfer in multiple scattering and emitting layered media, Appl. Opt., 27, 2502-2509, 1998.

675 Stephens, G. L.: The parameterization of radiation for numerical weather prediction and climate models, Mon Wea. Rev., 112, 826-867, 1984.

Stephens, G. L.: Cloud feedbacks in the climate system: A critical review, J. Clim., 18, 237-273, doi: 10.1175/JCLI-3243.1, 2005.

Stephens, G. L., and P. J. Webster: Clouds and climate: Sensitivity of simple systems, J. Atmos. Sci., 38, 235-247, 1981.

680 Stevens, B., and S. Bony: Water in the atmosphere, Physics Today, 66, 29-34, doi: 10.1063/PT.3.2009, 2013.

Stone, P. H.: The effect of large-scale eddies on climate change, J. Atmos. Sci., 30, 521-529, 1973.

Strauss, B., R. Meerkötter, B. Wissinger, P. Wendling, and M. Hess: On the regional climatic impact of contrails: Microphysical and radiative properties of contrails and natural cirrus clouds, Ann. Geophysicae, 15, 1457-1467, 1997.

Stuber, N., R. Sausen, and M. Ponater: Stratosphere adjusted radiative forcing calculations in a comprehensive climate

685 model, Theor. Appl. Climat., 68, 125-135, 2001.

Stuber, N., M. Ponater, and R. Sausen: Why radiative forcing might fail as a predictor of climate change, Clim. Dyn., 24, 497-510, doi: 10-1007/s00382-004-0497-7, 2005.

Vallis, G. K.: Atmospheric and Oceanic Fluid Dynamics, Cambridge Univ. Press, Cambridge, 2006.

Vázquez-Navarro, M., H. Mannstein, and S. Kox: Contrail life cycle and properties from 1 year of MSG/SEVIRI rapid-scan

690 images, Atmos. Chem. Phys., 15, 8739-8749, doi: 10.5194/acp-15-8739-2015, 2015.

Weihs, P., M. Rennhofer, D. J. Baumgartner, J. Gadermaier, J. E. Wagner, J. E. Gehring, and W. Laube: Potential impact of contrails on solar energy gain, Atmos. Meas. Tech., 8, 1089-1096, doi: 10.5194/amt-8-1089-2015, 2015.

Wendisch, M., P. Pilewskie, J. Pommier, S. Howard, P. Yang, A. J. Heymsfield, C. G. Schmitt, D. Baumgardner, and B. Mayer: Impact of cirrus crystal shape on solar spectral irradiance: A case study for subtropical cirrus, J. Geophys. Res., 110,
695   D03202, doi: 10.1029/2004JD005294, 2005.

Wetherald, R. T., and S. Manabe: The effects of doubling the CO2 concentration on the climate of a general circulation model, J. Atmos. Sci., 32, 3-15, 1975.

Wyser, K., and J. Ström: A possible change in cloud radiative forcing due to aircraft exhaust, Geophys. Res. Lett., 25, 1673-1676, 1998.

700   Yang, P., K. N. Liou, L. Bi, C. Liu, B. Q. Yi, and B. A. Baum: On the radiative properties of ice clouds: Light scattering, remote sensing, and radiation parameterization, Adv. Atmos. Sci., 32, 32–63, doi: 10.1007/s00376-014-0011-z, 2015.

Zhang, Y., A. Macke, and F. Albers: Effect of crystal size spectrum and crystal shape on stratiform cirrus radiative forcing, Atmos. Res., 52, 59-75, doi: 10.1016/S0169-8095(99)00026-5, 1999.

Zhu, X.: Radiative damping revisited: Parameterization of damping rate in the middle atmosphere, J. Atmos. Sci., 50, 3008-
705   3021, 1993.

Table 1. Radiative Forcing (RF)[*], surface temperature change ΔT_s, sensitivity parameters λ and efficacies e relative to adjusted and effective RF_a and RF_s, for contrail cirrus and CO_2 for the given model. The first four rows are the radiative cases with zero turbulent fluxes, the last four rows apply for the radiative-diffusive cases. The instantaneous and adjusted RF values are the same for both cases. Negative λ and e values are considered ill-conditioned because highly sensitive to small changes in forcing and mixing contributions.

	RF_i	$RF_{i,TOA}$	$RF_{i,SUR}$	RF_a	RF_s	ΔT_s	λ_a	λ_s	e_a	e_s	$RF_s/RF_{i,TOA}$
	W m^{-2}	W m^{-2}	W m^{-2}	W m^{-2}	W m^{-2}	K	K W^{-1} m^2	K W^{-1} m^2	1	1	1
					radiative case						
CO_2	0.83	0.41	0.07	0.72	0.26	0.12	0.16	0.45	1	1	0.64
SW Cirrus	-0.49	-0.48	-0.46	-0.49	-0.48	-0.22	0.44	0.44	2.69	0.99	1.00
LW Cirrus	0.92	0.88	0.09	0.90	0.20	0.09	0.10	0.45	0.60	0.99	0.23
Cirrus	0.43	0.40	-0.37	0.42	-0.28	-0.13	-0.30	0.44	-1.83	0.98	-0.70
					radiative-diffusive case						
CO_2	0.83	0.41	0.07	0.72	0.70	0.19	0.26	0.26	1	1	1.70
SW Cirrus	-0.49	-0.48	-0.46	-0.49	-0.49	-0.13	0.27	0.26	1.04	1.00	1.03
LW Cirrus	0.92	0.88	0.09	0.90	0.81	0.21	0.24	0.26	0.92	1.00	0.92
Cirrus	0.43	0.40	-0.37	0.42	0.32	0.08	0.20	0.26	0.79	1.00	0.79

[*] Index i for instantaneous values at tropopause (TP), top of atmosphere (TOA), and surface (SUR); a for adjusted at TP; and s for effective at TP.
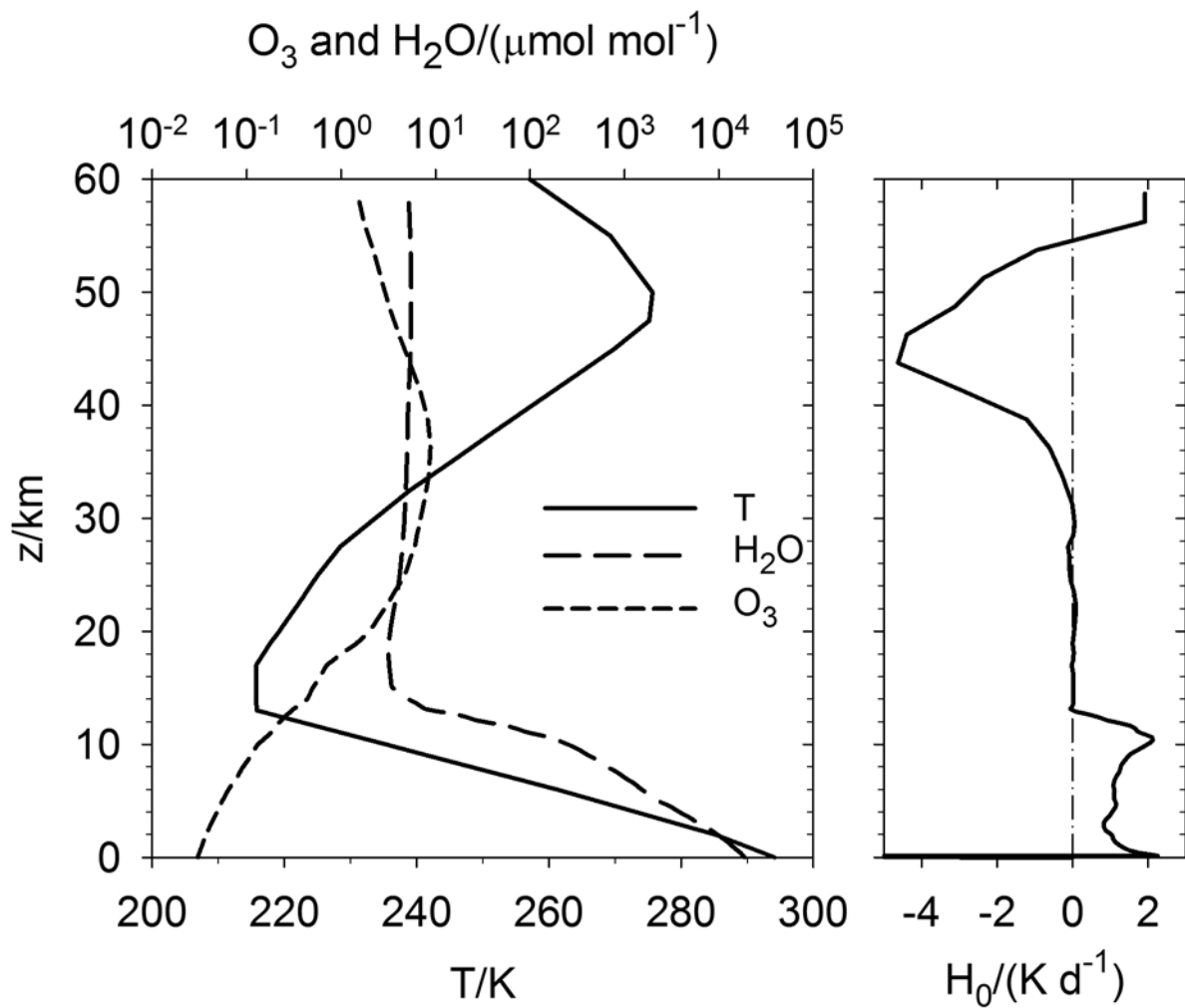
Figure 1. Temperature T of the mid-latitude summer standard atmosphere versus height z, together with water vapor and ozone molar mixing ratio (O_2: 0.2002 mol mol^{-1}; CO_2: 360 µmol mol^{-1}), and heating rate $H_0 = Q_0/(\rho\, c_p)$ keeping the atmosphere at steady-state. Because of TOA radiative imbalance, H_0 is strongly negative at the surface; in the mass-weighted average, $H_0 = -1.25$ K d^{-1} in the troposphere and -0.057 K d^{-1} in the stratosphere, balancing the summer warming.
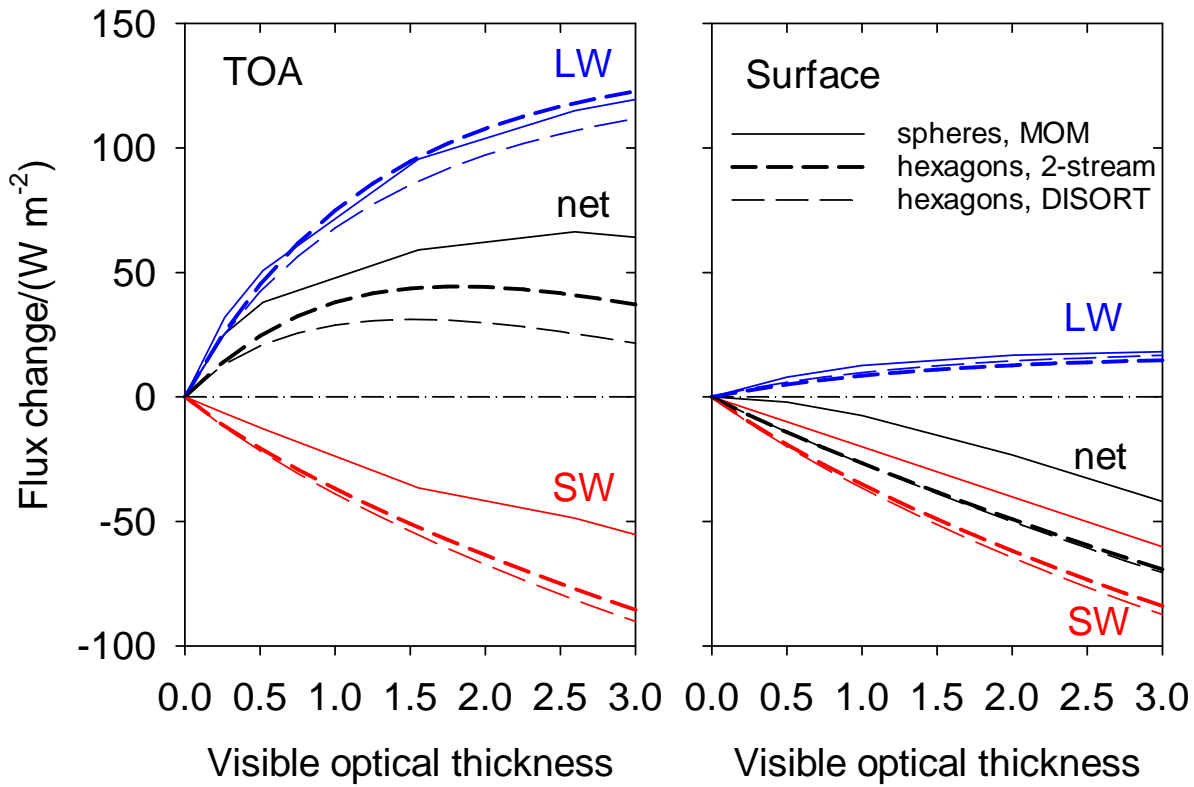
Figure 2. Day-mean cloud radiative effects from a homogeneous contrail layer at 10 to 11 km altitude versus 550-nm optical
thickness. The contrail cirrus is assumed to be composed of spheres (Meerkötter et al., 1999) or hexagons (Fu and Liou,
1993). The cloud radiative effect is the flux difference relative to the cloud-free atmosphere, and computed with matrix
operator method (MOM; Plass et al. (1973)), two-stream, and discrete ordinate (DISORT) solvers and the Fu & Liou
parametrization for molecular absorption, for daily mean at 45°N, 21 June, standard mid-latitude summer atmosphere, over a
surface with albedo 0.2, and fixed surface temperature (294.2 K). Differences between the SW (LW) fluxes from the two-
stream and DISORT solvers are < 6% (<19%).
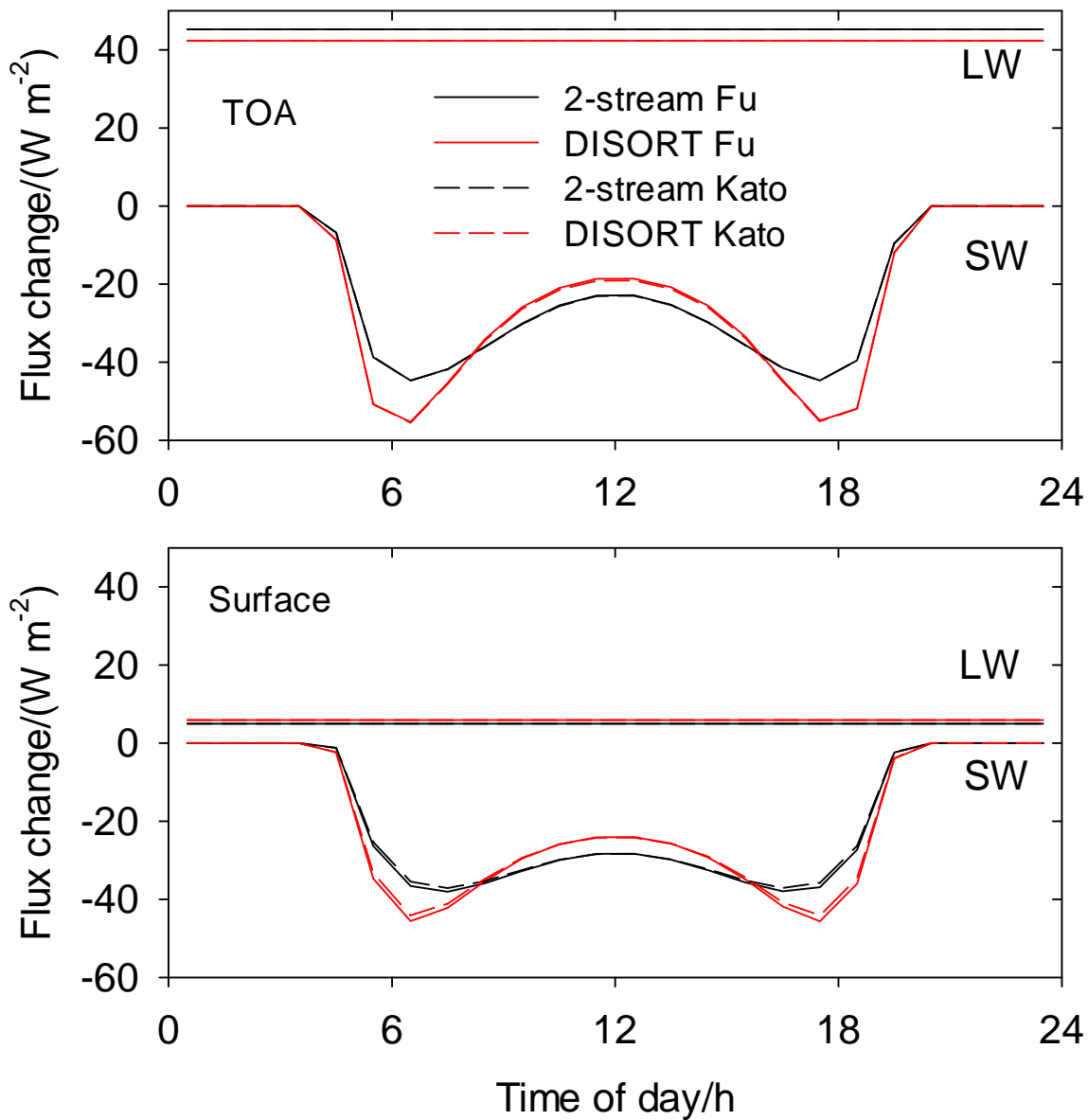
Figure 3. LW and SW flux changes versus time of day at TOA and at the surface, for two-stream and DISORT solvers, and for Fu & Liou and Kato shortwave molecular absorption parametrizations. The model parameters are the same as in Figure 735 2, τ =0.5. The flux differences for different molecular absorption models of Fu and Kato are far smaller than between the two-stream solver and DISORT.
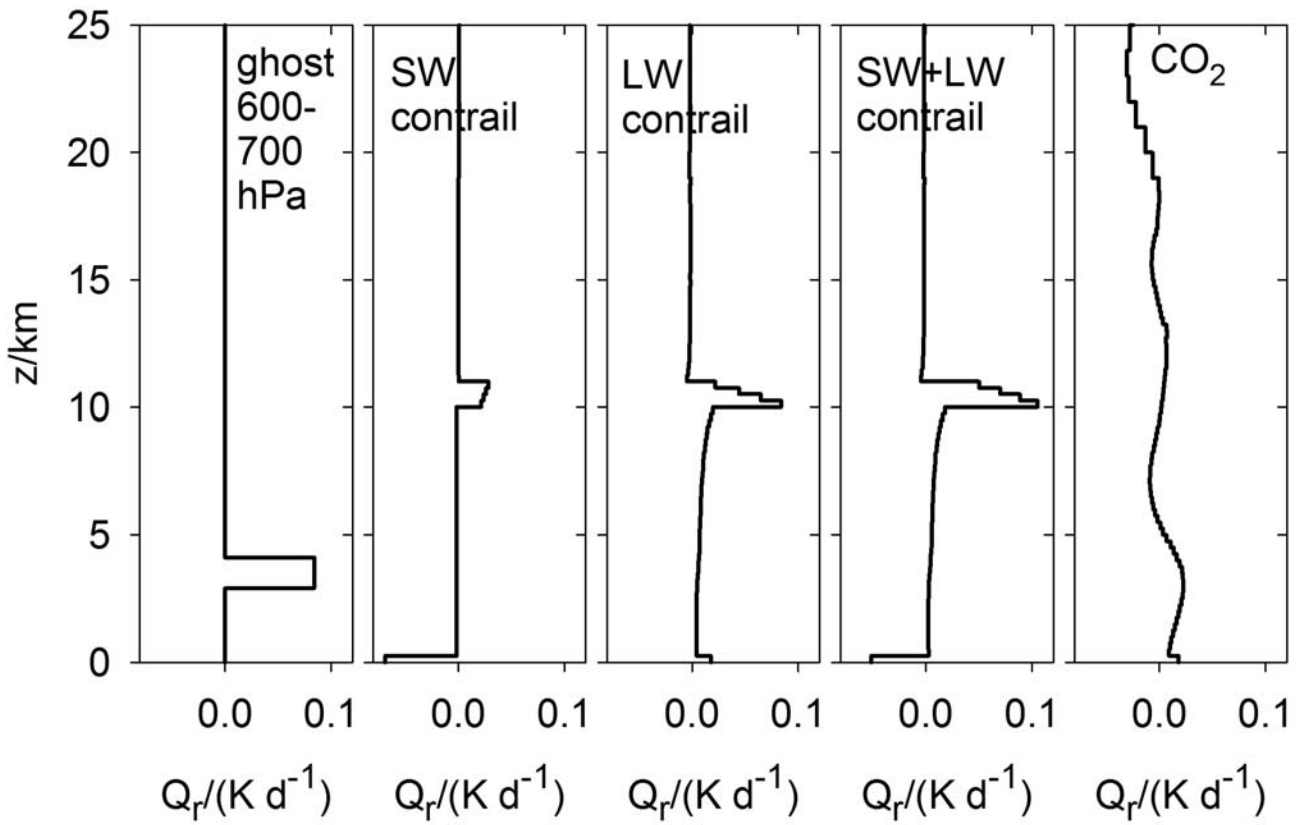
Figure 4: Initial radiative heating rates H(t=0, z) versus height z for a ghost forcing example, for SW, LW and SW+LW contrail cirrus, and for a CO_2 disturbance. For plotting, the local heating rate induced by the nonzero radiative fluxes at the fixed-temperature surface is distributed over the lowest 275 m height (same heat capacity as 1 km thick cirrus layer at lower pressure).
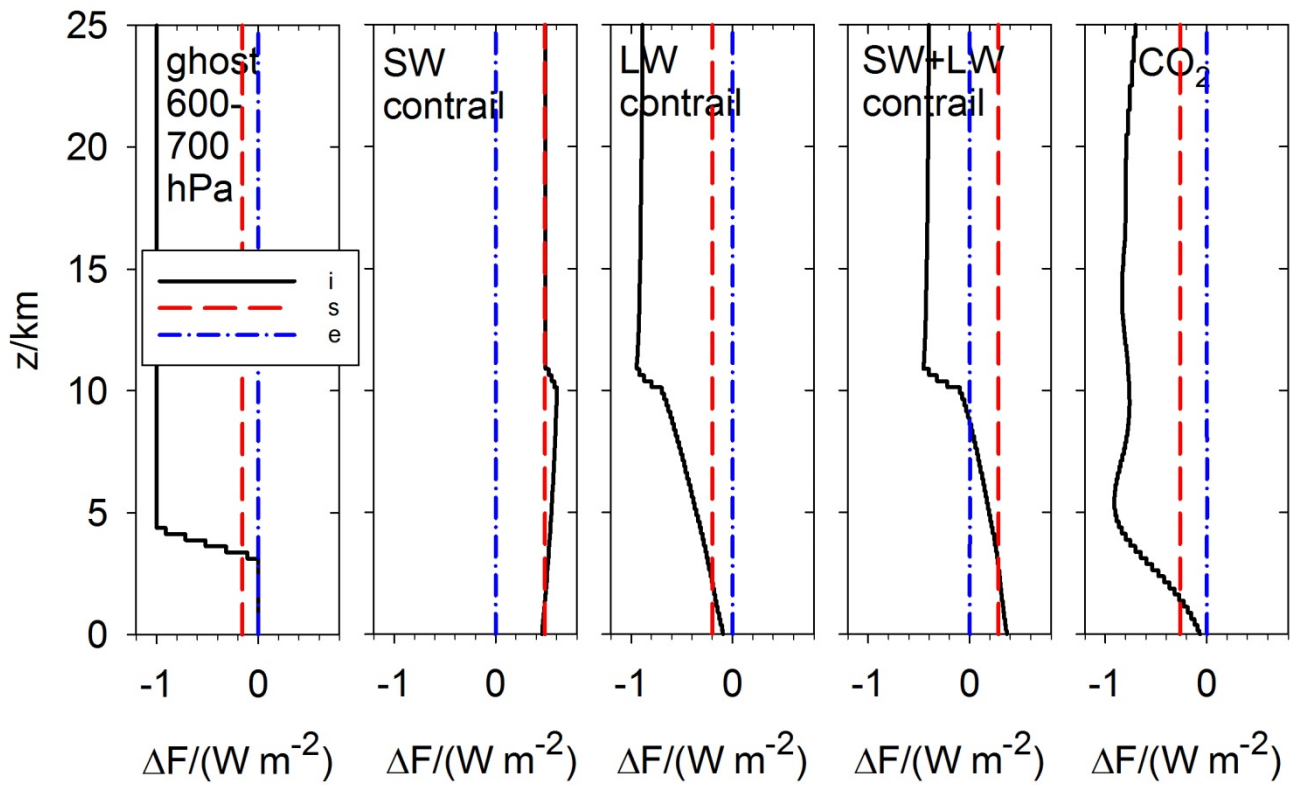
Figure 5. Initial and final radiative flux changes ΔF versus height z as induced by a disturbance from added ghost heating, SW, LW, and SW+LW contrail cirrus, and 10 % increased CO_2, in the panels from left to right, respectively. Black full lines (i): instantaneous flux; red dashed line (s): adjusted to constant surface temperature; blue dash-dotted line (e): equilibrium over adiabatic surface. The fluxes F are positive if upwards.
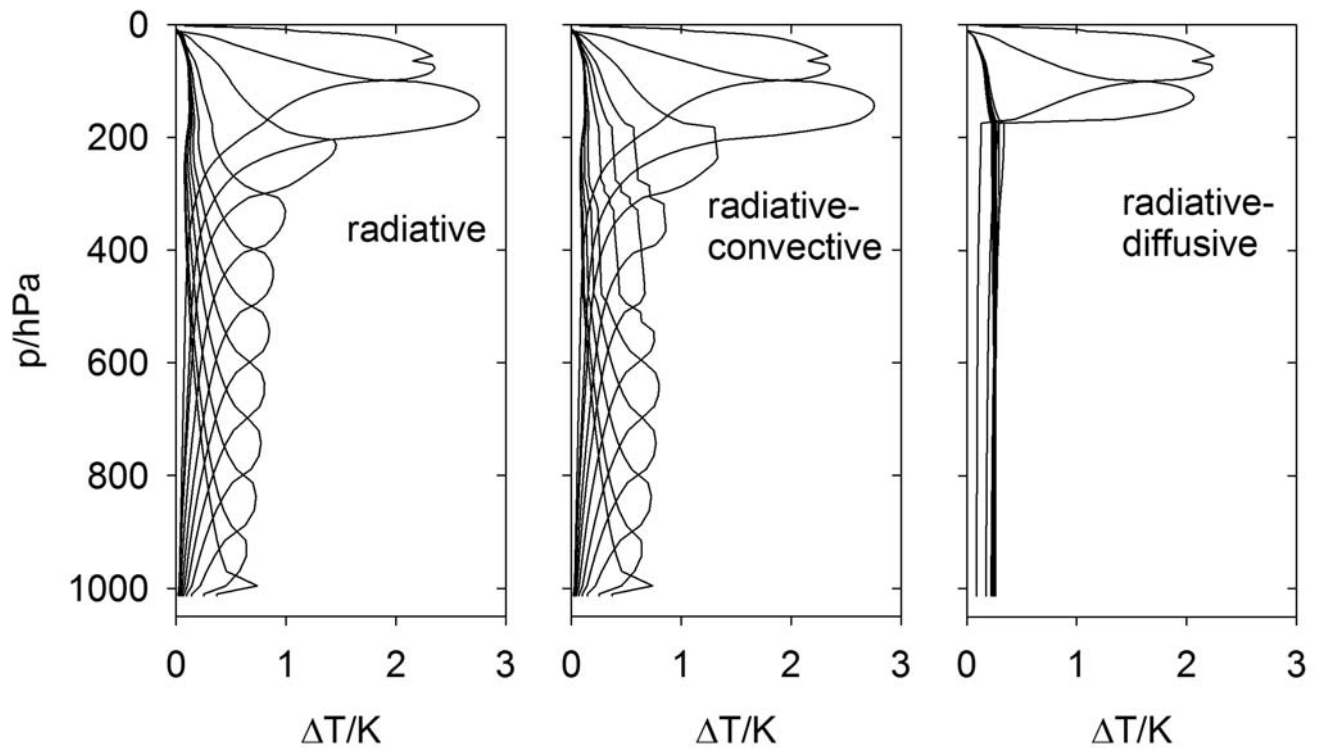
Figure 6: Temperature response versus pressure altitude for layer heating (ghost forcing) with 1 W m^{-2} in ten subsequent 100-hPa pressure layers and above an adiabatic surface. Left: the "radiative case" with zero turbulent fluxes; middle: the "radiative-convective case" with convective adjustment in addition to radiative energy transport; right: the "radiative-diffusive case" with diffusive mixing ($\kappa = 100$ m^2 s^{-1} in the troposphere, 0 in the stratosphere) in addition to radiative energy transport.
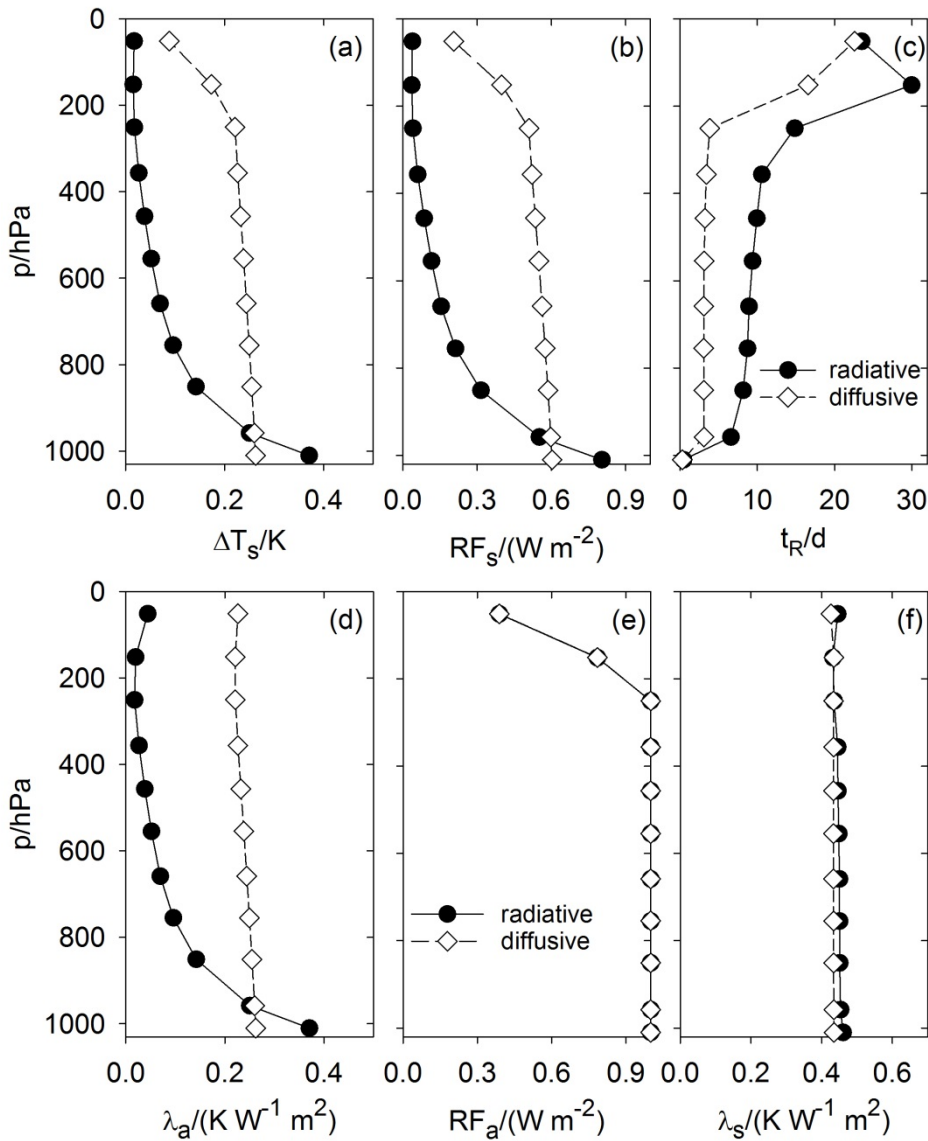
765 **Figure 7:** (a) Temperature change at the surface for layer heating versus the layer pressure height. The ghost forcing corresponds to an RF_i of 1 W m^{-2} at TOA. Black symbols with full line: radiative case; white symbols with dashed line: radiative-diffusive case. (b) Corresponding RF_s values for fixed T_s. (c) Relaxation time scales $t_R = \Delta T_{layer}/H$. (d) Climate sensitivity parameter $\lambda_a = \Delta T_s/RF_a$ based on stratosphere-adjusted RF_a; (e) RF_a; (f) climate sensitivity parameter $\lambda_s = \Delta T_s/RF_s$ based on effective RF_s.

770
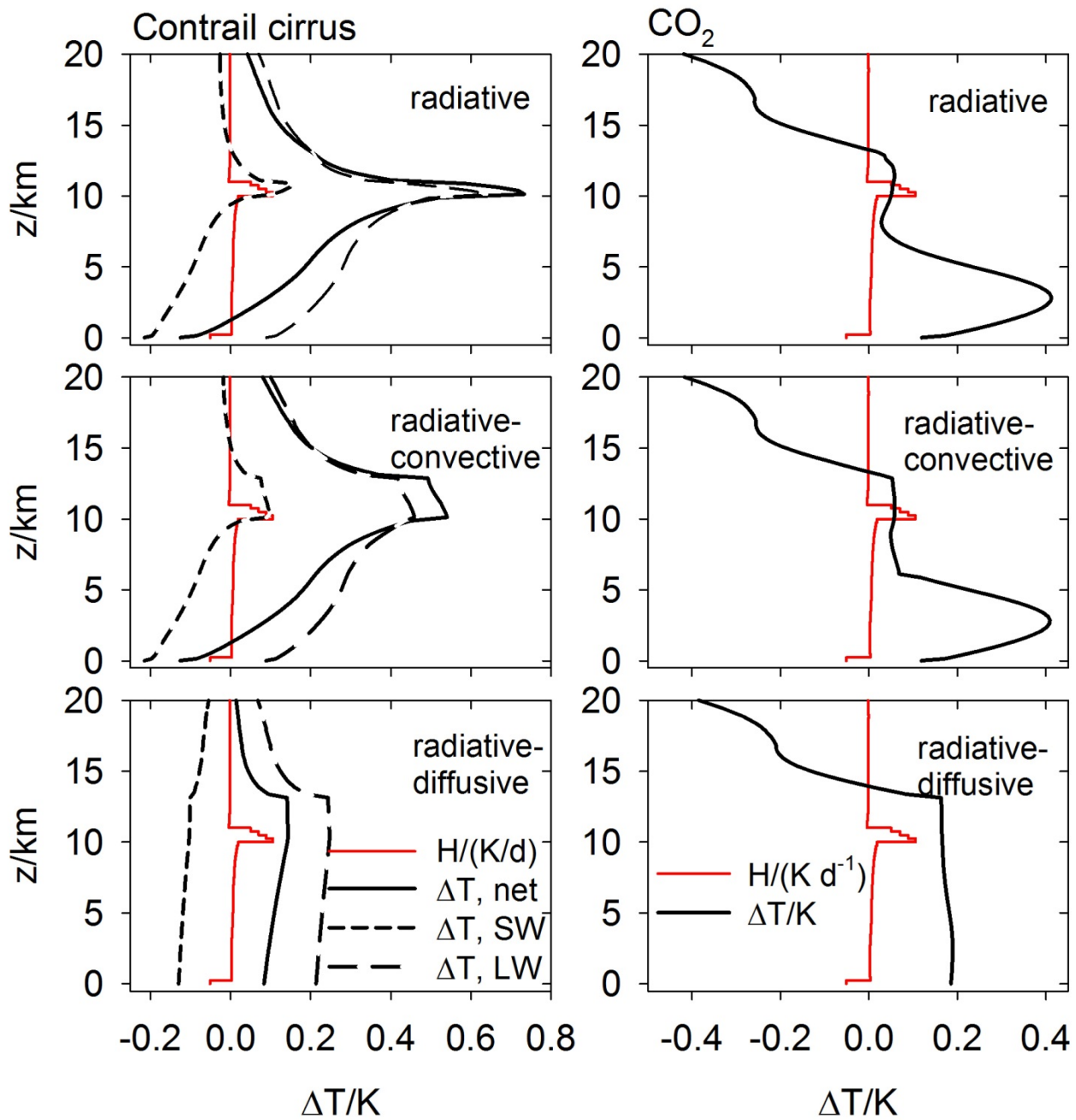
Figure 8: Temperature change ΔT in K versus altitude z in km (black lines) for disturbances by CO_2 (left) and by SW, LW and combined LW+SW contrail cirrus (right), in steady state for the radiative, radiative-convective and radiative-diffusive cases. The red curves show the net (LW+SW) initial instantaneous heating ratings in K d^{-1}.

775
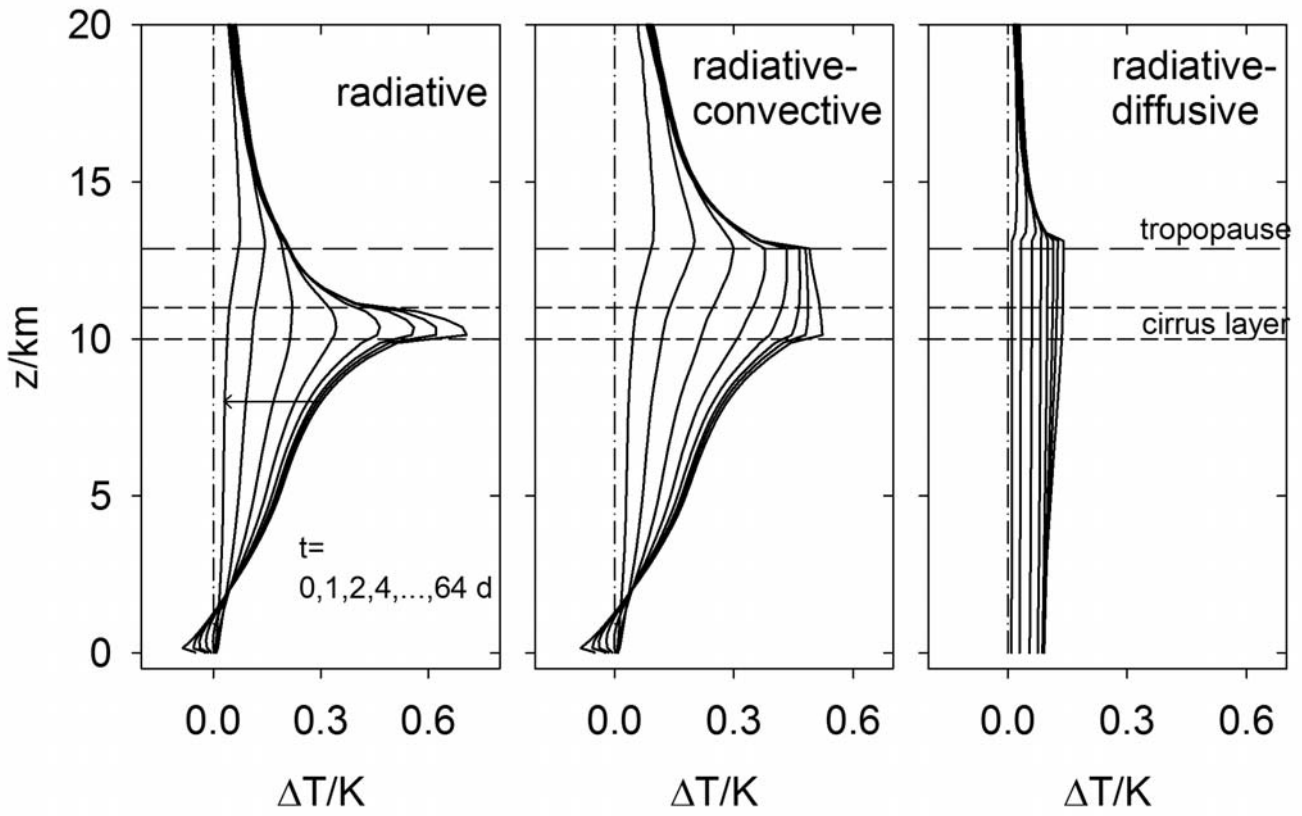
Figure 9. Decay of an initially steady-state contrail-cirrus-induced temperature increase, at times 0, 1, 2, 4, ..., 64 d after the contrail-cirrus ceased, in three panels for the radiative, radiative-convective and radiative-diffusive cases. Tropopause and

780   contrail layer heights are indicated by dashed lines.